

Water-Soluble Mono- and Binuclear Ru(η^6 -*p*-cymene) Complexes Containing Indole Thiosemicarbazones: Synthesis, DFT Modeling, Biomolecular Interactions, and *In Vitro* Anticancer Activity through Apoptosis

Jebiti Haribabu,[†] Gopal Sabapathi,[‡] Manoharan Muthu Tamizh,[§] Chandrasekar Balachandran,^{||} Nattamai S. P. Bhuvanesh,[⊥] Ponnambalam Venuvanalingam,[‡] and Ramasamy Karvembu^{*,†,||}

[†]Department of Chemistry, National Institute of Technology, Tiruchirappalli 620 015, India

[‡]Theoretical and Computational Chemistry Laboratory, School of Chemistry, Bharathidasan University, Tiruchirappalli 620 024, India

[§]Department of Chemistry, Siddha Central Research Institute, Central Council for Research in Siddha, Arumbakkam, Chennai 600 106, India

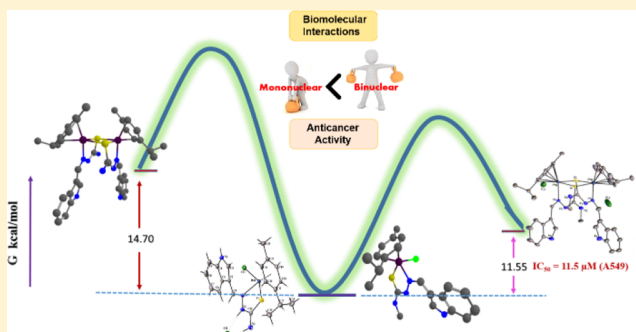
^{||}Division of Natural Drug Discovery, Institute of Natural Medicine, University of Toyama, 2630 Sugitani, Toyama 930-0194, Japan

[⊥]Department of Chemistry, Texas A&M University, College Station, Texas 77842, United States

Supporting Information

ABSTRACT: Indole thiosemicarbazone ligands were prepared from indole-3-carboxaldehyde and *N*-(un)substituted thiosemicarbazide. The Ru(η^6 -*p*-cymene) complexes [Ru(η^6 -*p*-cymene)(HL1)Cl]Cl (**1**) and [Ru(η^6 -*p*-cymene)(L2)]₂Cl₂ (**2***) were exclusively synthesized from thiosemicarbazone (TSC) ligands HL1 and HL2, and [RuCl₂(*p*-cymene)]₂. The compounds were characterized by analytical and various spectroscopic (electronic, FT-IR, 1D/2D NMR, and mass) tools. The exact structures of the compounds (HL1, HL2, **1**, and **2***) were confirmed by single-crystal X-ray diffraction technique. In complexes **1** and **2***, the ligand coordinated in a bidentate neutral (**1**)/monobasic (**2***) fashion to form a five-membered ring. The complexes showed a piano-stool geometry around the Ru ion. While **2*** existed as a dimer, **1** existed as a monomer, and this was well explained through free energy, bond parameter, and charge values computed at the B3LYP/SDD level.

The intercalative binding mode of the complexes with calf thymus DNA (CT DNA) was revealed by spectroscopic and viscometric studies. The DNA (pUC19 and pBR322 DNA) cleavage ability of these complexes evaluated by an agarose gel electrophoresis method confirmed significant DNA cleavage activity. Further, the interaction of the complexes with bovine serum albumin (BSA) was investigated using spectroscopic methods, which disclosed that the complexes could bind strongly with BSA. A hemolysis study with human erythrocytes revealed blood biocompatibility of the complexes. The *in vitro* anticancer activity of the compounds (HL1, HL2, **1**, and **2***) was screened against two cancer cell lines (A549 and HepG-2) and one normal cell line (L929). Interestingly, the binuclear complex **2*** showed superior activity with IC₅₀ = 11.5 μ M, which was lower than that of cisplatin against the A549 cancer cell line. The activity of the same complex (IC₅₀ = 35.3 μ M) was inferior to that of cisplatin in the HepG-2 cancer cell line. Further, the apoptosis mode of cell death in the cancer cell line was confirmed by using confocal microscopy and DNA fragmentation analysis.



INTRODUCTION

Since the discovery of cisplatin for medicinal purposes in 1979, it has been one of the most popular drugs and has established the importance of organometallic compounds in the pharmaceutical industry. The main cellular target of the drug is presumed to be DNA, particularly the construction of 1,2-intrastrand cross-link adducts forcing the DNA to curve toward the major groove. This leads to the deformation of DNA, which effectively blocks cell division and triggers cell death.^{1–3} Over the decades, analogues of cisplatin such as carboplatin,

oxaliplatin, tetraplatin, zeniplatin, enloplatin, etc. have been widely investigated for their *in vivo* interaction with DNA. Unfortunately, the clinical application of cisplatin is restricted due to the frequent development of drug resistance, limited range of tumors against which the drug is active, and also several side effects. Therefore, the search for the development

Received: January 4, 2018

of metal-based drugs with more efficiency, less toxicity, and target specificity is ongoing.^{4–9}

Since the approval of cisplatin for the treatment of cancer, a number of nonplatinum complexes has been studied for their chemotherapeutic potential.^{10–12} Among other metal compounds, ruthenium has gained preference due to its ability to mimic iron in natural biological processes and to show various oxidation states under physiological conditions.¹³ *Trans*-[RuCl₄(Im)(dmsO-S)]⁻ (NAMI-A, Im = imidazole) and *trans*-[RuCl₄(Ind)₂]⁻ (KP1019, Ind = 1*H*-indazole) are two ruthenium complexes that have moved past phase I clinical trials.^{14–16} NAMI-A has already been approved for a phase II clinical study.¹⁷ In 1992, Tocher and co-workers reported the first anticancer Ru(II)–arene complex, [Ru(η^6 -benzene)-(metronidazole)Cl₂].¹⁸ Sadler et al. have established the mechanism of action of their compounds of the type [Ru(η^6 -arene)(en)(Cl)]⁺, which have many analogies to the mechanism of cisplatin.¹⁹

Half-sandwich Ru(II)–arene complexes are currently attracting increasing interest as anticancer compounds. Recently developed Ru(II)–arene complexes containing a phosphine ligand, such as [Ru(η^6 -benzene)(pta)Cl₂] (RAPTA-B) and [Ru(η^6 -*p*-cymene)(pta)Cl₂] (RAPTA-C) (pta = 1,3,5-triaza-7-phosphaadamantane), show very promising *in vivo* activity on the inhibition of metastasis growth,²⁰ together with high selectivity and low general toxicity.²¹ The electronic and structural factors of the Ru(II)–arene complexes are known to play an important role in determining their biological activity, and hence efforts are ongoing to fine-tune their therapeutic ability by varying these factors systematically.²²

Over the years, thiosemicarbazones (TSCs) and their heterocyclic derivatives have captured attention in the pharmaceutical world due to their wide range of bioactivities.^{23,24} TSCs are known to possess three donor sites, two N atoms and one S atom, which coordinate with different metal ions to form stable complexes that have been reported to possess curative properties such as antifungal, antibacterial, antioxidant, antitumor, etc.^{25–28} Ru(II)–arene complexes bearing TSCs have been evolving as promising therapeutic agents.^{29–36} In general, in Ru(II)–arene complexes of TSCs, the ligand usually coordinates with the Ru(II) ion in the thione (C=S) form in a bidentate fashion with N¹,S donor atoms forming a five-membered chelate ring, resulting in mononuclear complexes.^{29–36} Even though there have been an impressive number of reports on Ru(II)–arene complexes with TSC ligands, just two reports have dealt with binuclear Ru(II)–arene complexes wherein TSC ligands show bidentate (N¹,S/N²,S) chelation to Ru(II) ion in the anionic form of thiolate, forming a five-/four-membered chelate ring (Figure 1).^{37,38}

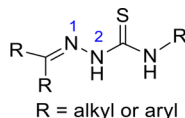


Figure 1. General structure of TSC ligands.

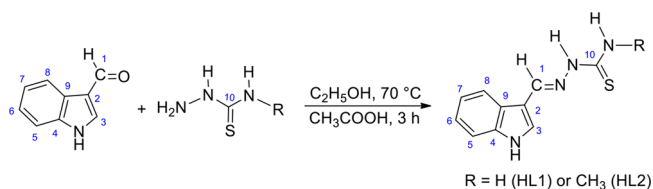
For a long time, reports on Ru(II)–arene complexes with TSCs have appeared in the literature due to their significant biological properties. The study of these complexes based on their mode of action and their interaction with biological targets is still an active research topic. These factors motivated us to develop water-soluble mono- and binuclear Ru(η^6 -*p*-cymene)

complexes containing indole-based TSC ligands and evaluate their biomolecular interactions, DNA cleavage, hemolysis, and anticancer activity.

RESULTS AND DISCUSSION

Synthesis of the Ligands and Complexes. Indole TSCs (HL1 and HL2) were synthesized by the condensation of thiosemicarbazide/4-methylthiosemicarbazide with indole-3-carboxaldehyde in the presence of acetic acid (Scheme 1),

Scheme 1. Synthetic Scheme of the Indole TSC Ligands

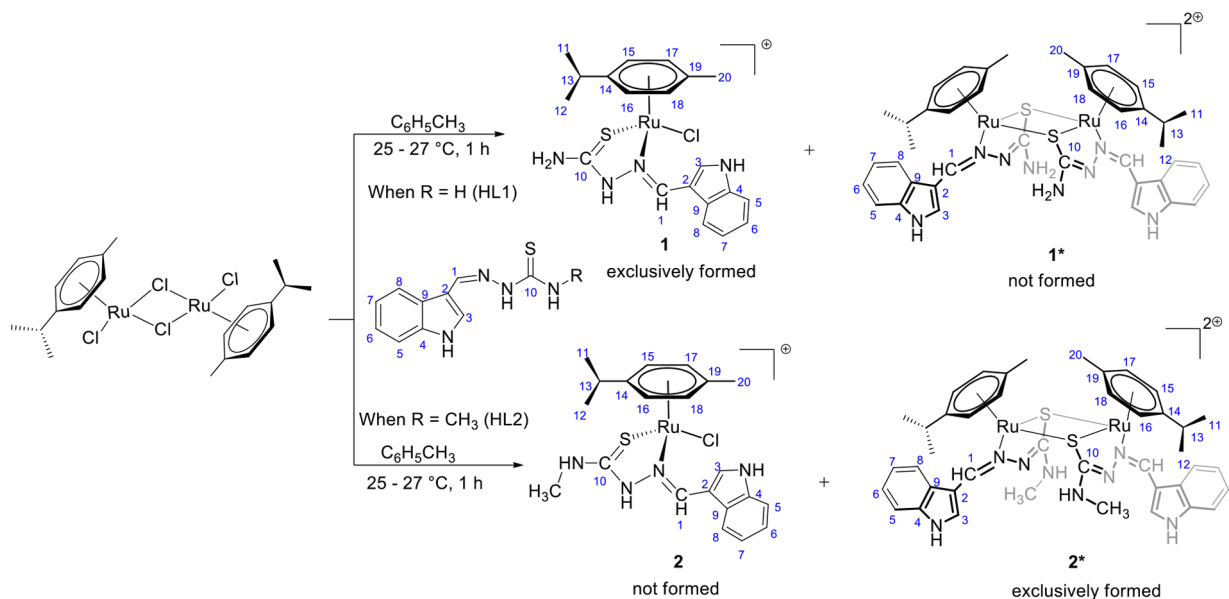


and their corresponding Ru(η^6 -*p*-cymene) complexes were synthesized using [RuCl₂(*p*-cymene)]₂ as a precursor (Scheme 2). The reaction between TSC ligands and [RuCl₂(*p*-cymene)]₂ was expected to yield either mono- or binuclear Ru(η^6 -*p*-cymene) complexes.^{37,38} Li and co-workers prepared binuclear Ru(II)–arene complexes of TSC ligands from the corresponding mononuclear complexes.³⁸ In our case, interestingly, formation of a mono- or binuclear complex depended on the substituent on the terminal nitrogen of the ligand. The factors favoring the dimerization were revealed from DFT studies. The complexes (1 and 2*) were air and light stable and soluble in water and most organic solvents. The ligands and complexes were characterized by CHNS analyses and various spectroscopic tools. The analytical data of the ligands and their complexes were in good agreement with the suggested molecular formula. The crystal structures of the compounds (HL1, HL2, 1, and 2*) were determined.

Confirmation of the Formation of the Ligands and Complexes. The UV–visible spectra of the ligands exhibited two bands in the regions 262–264 and 329–330 nm, which corresponded to intraligand ($\pi \rightarrow \pi^*$ and $n \rightarrow \pi^*$) transitions. The spectra of the complexes showed three bands. Two bands were seen in the 267–271 and 339–342 nm regions, which corresponded to $\pi \rightarrow \pi^*$ and $n \rightarrow \pi^*$ transitions, respectively. The third band observed at 429–432 nm corresponded to a $d \rightarrow d$ transition.³⁹

The FT-IR spectra of the ligands showed three bands in the range 3448–3440, 3325–3312, and 3238–3230 cm⁻¹, which were assigned to indole N–H, terminal N–H, and thiocarbonyl-attached N–H bonds, respectively. The azomethine (C=N) and thiocarbonyl (C=S) stretching frequencies of the ligands were observed at 1551–1548 and 1299–1295 cm⁻¹, respectively. On complexation, there was a decrease in C=N (1503–1501 cm⁻¹) and C=S (1244–1230 cm⁻¹) stretching frequencies. The shift in these bands suggested that the TSC ligands coordinated to Ru(II) ion through azomethine nitrogen (N¹) and thiocarbonyl sulfur.^{38,40}

In the ¹H NMR spectra of the ligands, signals due to indole N–H and thiocarbonyl-attached N–H protons appeared at 11.59 and 11.16 ppm, respectively. The signals due to protons of azomethine CH and indole CH were observed at 8.29–8.31 and 7.80 ppm, respectively. The protons of NH₂ in the ligand (HL1) resonated at 8.00 and 7.40 ppm as broad singlets. The terminal N–H proton in the ligand (HL2) was observed as a

Scheme 2. Synthetic Scheme of the Ru(η^6 -*p*-cymene) Complexes

quartet at 7.90 ppm. Further, a doublet appeared at 3.08 ppm in the spectrum of HL2, corresponding to the terminal CH₃ protons. In the ¹H NMR spectra of complexes **1** and **2***, indole N–H, azomethine C–H, and indole C–H protons gave signals at 11.80–11.83, 9.00–9.01, and 8.79–8.94 ppm, respectively. The isopropyl methyl protons in *p*-cymene were shielded and resonated at 1.04–1.13 ppm. The *p*-cymene aromatic protons were also shielded and gave four different chemical shift values in the regions 5.69–5.72, 5.31–5.35, 5.26–5.27, and 5.17–5.21 ppm.³⁸ Assignment for individual aromatic protons has been made on the basis of ¹H–¹H correlation (COSY), ¹H–¹³C heteronuclear single quantum coherence (HSQC), and ¹H–¹³C heteronuclear multiple bond correlation (HMBC) spectra. The ¹H–¹H nuclear Overhauser (NOESY) spectrum of **1** yielded a through-space correlation between the CH proton of the indole ring and methyl protons in *p*-cymene (Figure S7). A similar interaction was also observed in complex **2*** (Figure S8). In the ¹³C NMR spectra of the ligands, the C=S and C=N carbons were observed in the regions 176.51–176.77 and 140.43–141.78 ppm, respectively. However, in the spectra of the complexes, the C=S (**1**)/C–S (**2***) and C=N carbons were observed at 176.76–179.08 and 155.05–156.91 ppm, respectively. The new carbon signals at 104.27–104.67, 89.47–89.83, 85.64–85.76, 84.36–84.87, 32.22–32.24, 23.16–23.26, 21.76–21.77, and 18.84–18.85 ppm were due to the *p*-cymene moiety in the complexes.^{38,41} All other protons/carbons resonated in the expected regions. The 1D/2D NMR spectra of the compounds are shown in Figures S1–S19.

Crystal Structure of the Ligands and Complexes. The crystal structures of compounds HL1, HL2, **1**, and **2*** are shown in Figures 2–5 respectively. Experimental details, bond distances, and bond angles are given in Tables 1 and 2 and Tables S1–S3. Suitable yellowish white crystals of the ligands were grown from solutions prepared from an acetonitrile and methanol mixture (1/1). The important torsion angles in ligands HL1 and HL2 were –178.40(11) (N(3)–N(2)–C(1)–S(1)), 0.5(2) (N(3)–N(2)–C(1)–N(1)), and –178.93(14)° (C(1)–N(2)–N(3)–C(2)) and 178.47(8) (N(2)–N(3)–C(10)–S(1)), 0.57(17) (N(2)–N(3)–C(10)–N(4)), 178.30(10) (N(3)–N(2)–C(9)–C(2)), –178.03(11)

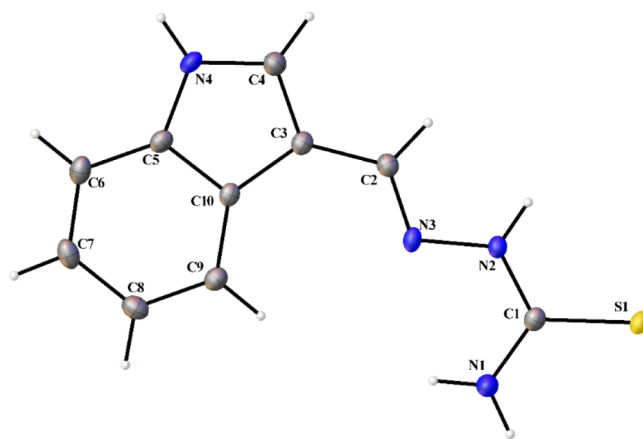


Figure 2. Thermal ellipsoid (50% probability) plot of HL1.

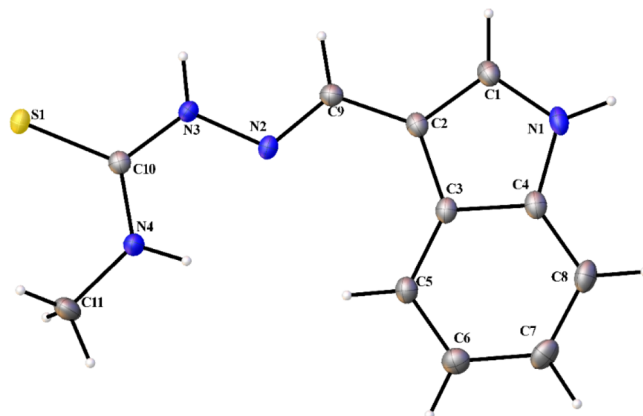


Figure 3. Thermal ellipsoid (50% probability) plot of HL2.

(C(9)–N(2)–N(3)–C(10)), 6.95(18) (C(11)–N(4)–C(10)–S(1)), and –175.20(12)° (C(11)–N(4)–C(10)–N(3)) respectively.²⁸ The S(1)–C(1/10), N(1)–C(1), and N(2)–N(3) bond lengths were 1.6965(16)–1.7010(13), 1.328(2)–1.3599(17), and 1.3839(18)–1.3841(14) Å in HL1

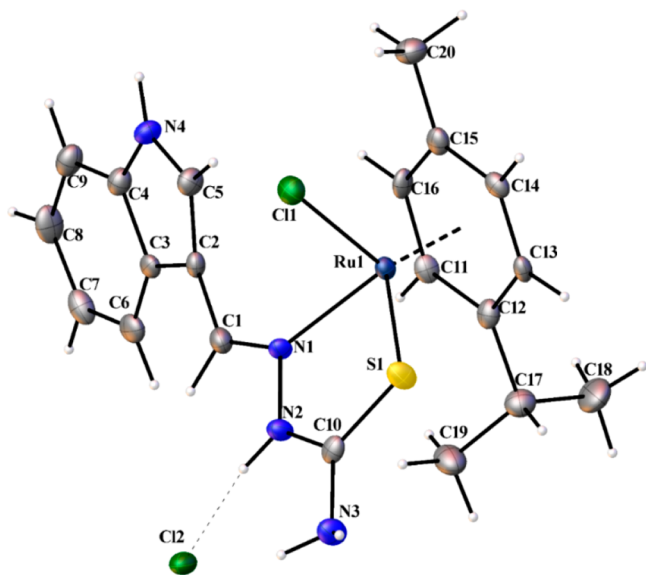


Figure 4. Thermal ellipsoid (50% probability) plot of **1**.

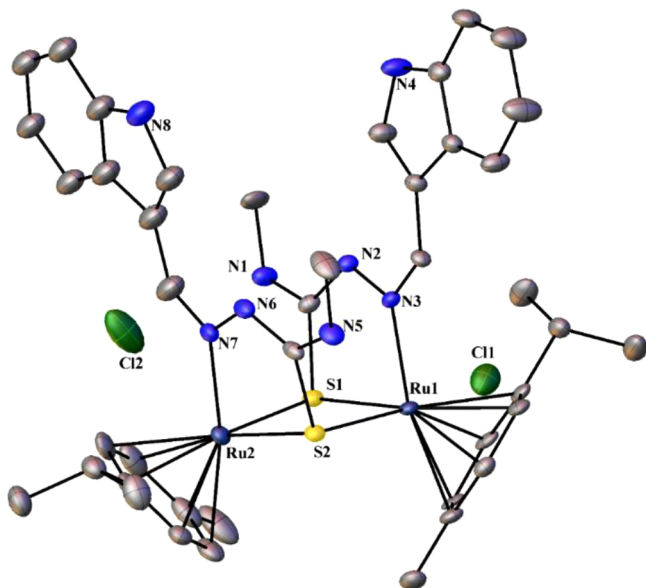


Figure 5. Thermal ellipsoid (50% probability) plot of **2***. Hydrogen atoms are not shown for clarity.

and HL2. The bond lengths and angles were comparable to those of a similar compound.^{42a}

Complex **1** crystallized in the monoclinic space group $P2_1$ with $Z = 2$ and adopted the familiar “three-legged piano-stool” geometry with the Ru(II) center being coordinated by a *p*-cymene, terminal chloride, and chelating N^1,S ligand (Figure 4). In complex **1**, the *p*-cymene was essentially planar, and the distance between the Ru(II) ion and the centroid of the aromatic ring was 2.203 Å.³¹ The bond distances around the Ru(II) ion varied over a small range (Ru–S, 2.3867 Å; Ru–N, 2.133 Å; Ru–Cl, 2.4036 Å), which were comparable to those of similar complexes.^{42b,43,44} The Cl[−] counterion involved in N(2)–H(2)⋯Cl(2) (3.061 Å), N(3)–H(3A)⋯Cl(2) (3.227 Å), and N(4)–H(4)⋯Cl(2) (3.103 Å) hydrogen-bonding interactions. The torsional angles in **1** were $-12.6(5)^\circ$ (Ru(1)–S(1)–C(10)–N(2)), $165.3(4)^\circ$ (Ru(1)–S(1)–C(10)–N(3)), and $10.6(6)^\circ$ (Ru(1)–N(1)–N(2)–C(10)).

Complex **2*** crystallized in the monoclinic space group $P2_1/n$ with $Z = 4$ and adopted a piano-stool shape with two molecules of L2 coordinated (N^1,S) to Ru(II) ion as a monoanionic bidentate ligand. Two $[(\eta^6\text{-}p\text{-cymene})\text{Ru}(\text{L}2)]^+$ moieties were held together by two bridging sulfur atoms of L2, adopting a binuclear structure with Ru_2S_2 core (Figure 5). The four-membered ring with bond angles of $81.71(5)^\circ$ (S(1)–Ru(1)–S(2)) and $81.70(5)^\circ$ (S(2)–Ru(2)–S(1)) was not planar. This kind of binuclear Ru(II)–arene complex is quite rare in comparison to similar reported complexes containing TSC ligands with N^2,S coordination mode.³⁸ The distance between the Ru(II) ion and centroid of the *p*-cymene ligand was 2.22 Å. The bond distances in **2***, 2.3519 (Ru(1)–S(1)), 2.4069 (Ru(1)–S(2)), 2.4133 (Ru(2)–S(1)), 2.3456 (Ru(2)–S(2)), 2.093 (Ru(1)–N(3)), and 2.090 Å (Ru(2)–N(7)), were comparable to those reported for similar compounds.^{31,37,38} The torsion angles Ru(1)–S(1)–C(1)–N(1), Ru(1)–S(1)–C(1)–N(2), Ru(1)–S(2)–C(22)–N(5), Ru(1)–S(2)–C(22)–N(6), Ru(2)–S(1)–C(1)–N(1), Ru(2)–S(1)–C(1)–N(2), Ru(2)–S(2)–C(22)–N(5), and Ru(2)–S(2)–C(22)–N(6) in **2*** were $173.0(4)^\circ$, $-6.2(5)^\circ$, $-87.2(4)^\circ$, $92.7(5)^\circ$, $-86.6(4)^\circ$, $94.2(5)^\circ$, $172.2(4)^\circ$, and $-8.0(5)^\circ$, respectively.

Dimerization. While **2*** existed as a dimer, **1** existed as a monomer. Structurally HL2 was different from HL1 only by a methyl group substituted on the terminal nitrogen atom, and this could have exerted a mild electronic effect so that complex **2** readily dimerized to **2***. To understand this, DFT calculations have been performed on the monomers (**1** and **2**) and dimers (**1*** and **2***). Their electronic structures and free energies were compared and analyzed. The optimized ground state geometries of **1**, **2**, **1***, and **2*** are given in Figure 6, and free energy changes during dimerization are given in Figure 7. The calculated geometrical parameters such as bond distances and angles are summarized in Table 2. Mulliken charge and bond order values are shown in Table 3. The free energy values for dimerization of **1** and **2** revealed that the process was endergonic in both cases but was less endergonic by 3.15 kcal/mol for **2** in comparison to **1**. This could explain why **2** existed as a dimer while **1** was a monomer. A similar observation was reported by Su et al.³⁸ This mild change in free energy could have been effected by the methyl group on the terminal nitrogen atom present in **2**. This can be well understood by examining the charge on the sulfur atom and the C–S bond length and bond order. The charge on sulfur in **2** was higher than that in **1**, and this was due to a push of electron density by the methyl group through the amino nitrogen atom. This enabled the sulfur atom to make the new S–Ru2 bond, resulting in dimer formation. Second, the bond order and length of the C–S bond in **1** and **2** were compared. The C–S bond was a partial double bond in the monomers, while it was a single bond in the dimers. In **2**, the double-bond character was slightly lower than in **1** and this enabled the C–S double bond to cleave easily in **2**. This also facilitated the dimerization of **2** over **1**. The computed and experimental bond parameters (Table 2) agreed well, and smaller deviations could be explained as due to crystal-packing effects.

DNA Binding Studies. *Hypochromism in the UV–Vis Absorption Spectra.* The changes observed in the absorption spectra of the complexes due to increasing concentration of CT DNA are used for determining the DNA binding ability of the complexes (Figure 8). The binding constant (K_b) values for the interaction of **1** and **2*** with CT DNA were 2.47×10^5 and 3.73×10^5 M, respectively (Table 4), which have been calculated

Table 1. Crystallographic Data and Refinement Parameters for HL1, HL2, 1, and 2*

parameter	HL1	HL2	1	2*
empirical formula	C ₁₀ H ₁₀ N ₄ S	C ₁₁ H ₁₂ N ₄ S	C ₂₀ H ₂₄ Cl ₂ N ₄ RuS	C ₄₅ H ₅₇ Cl ₂ N ₄ Ru ₂ S ₂
formula wt	218.28	232.31	524.46	1077.15
temp (K)	0.71073	0.71073	0.71073	1.54178
wavelength (Å)	tridinic	monoclinic	monoclinic	monoclinic
cryst syst	$P\bar{1}$	$P12_1/c1$	$P12_1$	$P12_1/n1$
space group				
unit cell dimens				
<i>a</i> (Å)	7.152(2)	13.3397(18)	9.2786(5)	13.9715(5)
<i>b</i> (Å)	11.128(3)	5.1353(7)	9.0809(4)	27.0092(8)
<i>c</i> (Å)	13.491(4)	16.016(2)	13.0911(6)	14.7779(5)
α (deg)	68.678(2)	90	90	90
β (deg)	85.059(3)	101.308(10)	104.855(6)	116.390(2)
γ (deg)	82.513(2)	90	90	90
<i>V</i> (Å ³)	990.8(5)	1075.8	1066.1(9)	4995.4(3)
<i>Z</i>	4	4	2	4
calcd density (Mg/m ³)	1.463	1.434	1.634	1.432
abs coeff (mm ⁻¹)	0.295	0.277	1.098	6.995
<i>F</i> (000)	456	488	532	2208
cryst size (mm ³)	0.54 × 0.32 × 0.3	0.52 × 0.43 × 0.41	0.34 × 0.09 × 0.04	0.06 × 0.04 × 0.02
θ range for data collection (deg)	1.622–27.39	2.59–27.55	2.27–27.43	3.27–60.88
index ranges	$-9 \leq h \leq 9, -14 \leq k \leq 14, -17 \leq l \leq 17$	$-17 \leq h \leq 17, -6 \leq k \leq 6, -20 \leq l \leq 20$	$-11 \leq h \leq 11, 0 \leq k \leq 11, 0 \leq l \leq 16$	$-15 \leq h \leq 15, -30 \leq k \leq 30, -16 \leq l \leq 16$
no. of rflns collected	11377	11778	3546	62224
no. of indep rflns (<i>R</i> (int))	4429 (0.0290)	2466 (0.0333)	3546	7440 (0.1478)
completeness to $\theta = 25.24^\circ$ (%)	99.6	99.3	98.5	82.2
abs cor				
max and min transmission	0.7456 and 0.6569	0.7456 and 0.6155	semiempirical from equivalents	0.7519 and 0.5713
refinement method			full-matrix least squares on <i>F</i> ²	
no. of data/restraints/params	4429/0/271	2466/0/146	3546/1/258	7440/779/544
goodness of fit on <i>F</i> ²	1.057	1.048	1.048	1.080
final <i>R</i> indices (<i>I</i> > 2 σ (<i>I</i>))	<i>R</i> 1 = 0.0362, <i>wR</i> 2 = 0.0898	<i>R</i> 1 = 0.0322, <i>wR</i> 2 = 0.0834	<i>R</i> 1 = 0.0270, <i>wR</i> 2 = 0.0587	<i>R</i> 1 = 0.0501, <i>wR</i> 2 = 0.1329
<i>R</i> indices (all data)	<i>R</i> 1 = 0.0429, <i>wR</i> 2 = 0.0932	<i>R</i> 1 = 0.0341, <i>wR</i> 2 = 0.0847	<i>R</i> 1 = 0.0286, <i>wR</i> 2 = 0.0596	<i>R</i> 1 = 0.0633, <i>wR</i> 2 = 0.1417
largest diff peak and hole (e Å ⁻³)	0.318 and -0.302	0.354 and -0.380	0.469 and -0.497	2.225 and -1.026

Table 2. Selected Bond Lengths (Å) and Angles (deg) of the Optimized Complexes Computed at the B3LYP/SDD[#] (#SDD for Ru, 6-311g (d, p) for Other Atoms) Level

	exptl		calcd			
	1	2*	1	1*	2	2*
Ru–centroid	2.260	2.282	2.252	2.283	2.251	2.283
Ru(1)–S(1)	2.387	2.352	2.402	2.384	2.397	2.385
Ru(1)–S(2)		2.407		2.457		2.454
Ru(1)–Cl(1)	2.404		2.468		2.470	
Ru(1)–N(1)/(3)	2.133	2.093	2.128	2.121	2.128	2.121
Ru(2)–S(1)		2.413		2.384		2.454
Ru(2)–S(2)		2.346		2.457		2.384
Ru(2)–N(7)		2.090		2.121		2.121
C(10)/(1)–S(1)	1.703	1.792	1.698	1.810	1.704	1.816
S(1)–Ru(1)–S(2)		81.7		81.1		81.1
S(1)–Ru(1)–Cl(1)	89.4		88.1		88.3	
N(1)–Ru(1)–Cl(1)	88.9		83.9		83.9	
N(1)/(3)–Ru(1)–S(1)	80.9	80.6	81.0	80.1	81.2	80.2
N(3)–Ru(1)–S(2)		92.0		92.1		92.1
S(2)–Ru(2)–S(1)		81.7		81.1		81.1
N(7)–Ru(2)–S(1)		91.0		92.1		92.1
N(7)–Ru(2)–S(2)		80.5		80.1		80.2
Ru(1)–S(1)–Ru(2)		97.8		98.8		98.8
Ru(2)–S(2)–Ru(1)		98.2		98.8		98.8
N(6)–N(7)–Ru(2)		122.5		121.0		121.3

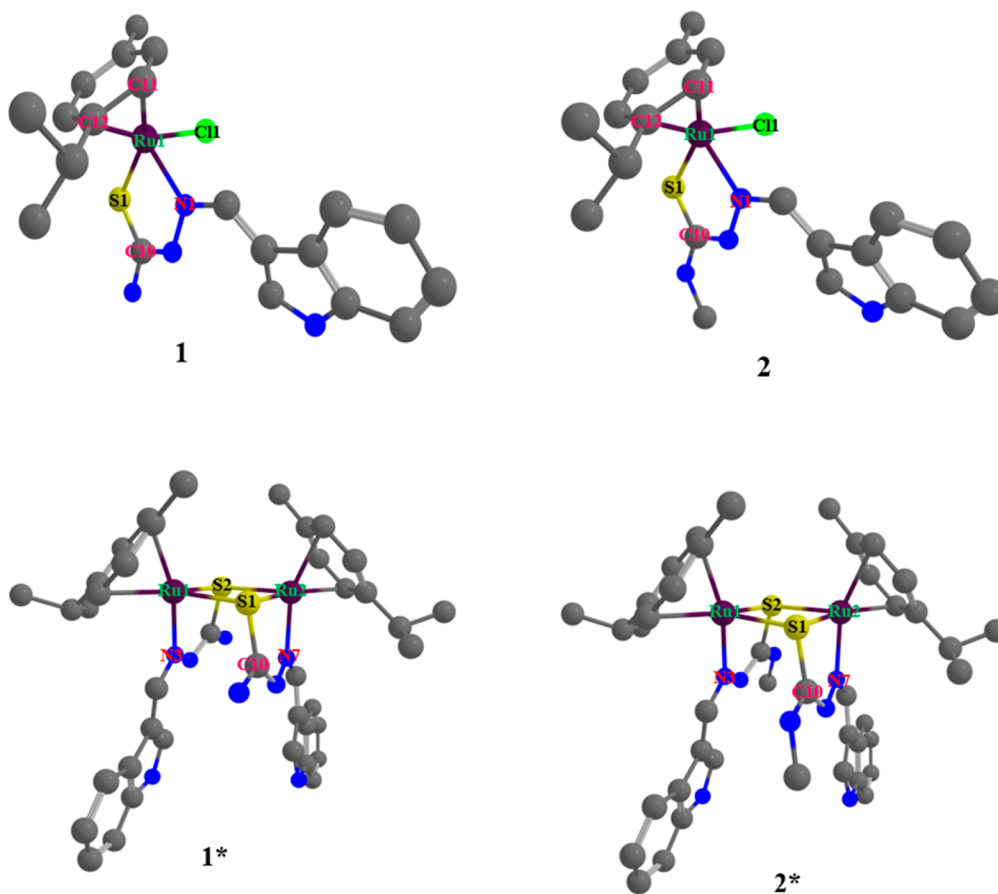


Figure 6. Optimized geometries of the complexes.

from the equation $[\text{DNA}]/(\epsilon_a - \epsilon_f) = [\text{DNA}]/(\epsilon_b - \epsilon_f) + 1/K_b$ ($\epsilon_b - \epsilon_f$), where $[\text{DNA}]$ is the concentration of CT DNA, ϵ_a , ϵ_f and ϵ_b correspond to $A_{\text{obsd}}/[\text{compound}]$, the extinction coefficient for the free compound, and the extinction coefficient

for the compound in the fully bound form, respectively (Figure 9).⁴⁵ The slope and intercept of $[\text{DNA}]/(\epsilon_a - \epsilon_f)$ versus $[\text{DNA}]$ plot gave $1/(\epsilon_b - \epsilon_f)$ and $1/K_b(\epsilon_b - \epsilon_f)$, respectively. Fixed amounts of the test compounds in DMF/Tris-HCl (15

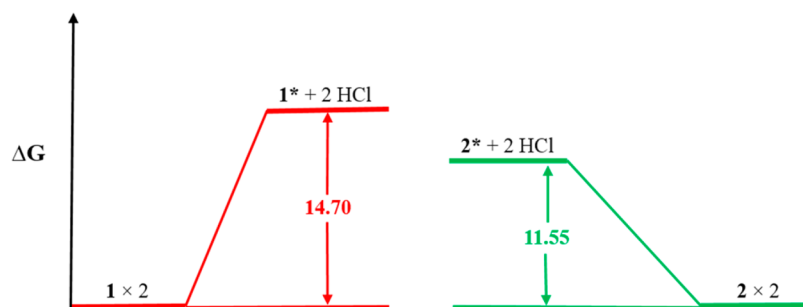


Figure 7. Gibbs free energy (kcal/mol) profile for $2 \times$ monomer (**1** and **2**) to dimer (**1*** and **2***) + 2 HCl.

Table 3. Data Obtained from the DFT Calculations on the Complexes

complex	Mulliken charge ^a			bond order		
	Ru	S	C	C=S	Ru1-S	Ru2-S
1	0.591	-0.023	0.202	1.407	0.502	
2	0.597	-0.042	0.206	1.381	0.507	
1*	0.541	-0.011	0.107	0.951	0.634	0.479
2*	0.557	-0.024	0.134	0.949	0.637	0.479

^aUnits in electrons.

μM) were used for titrations. In the absorption spectrum of complex **1**, the band at 342 nm showed a significant hypochromism with small red shift (3 nm) upon the addition of CT DNA (0–35 μM). During the incremental addition of CT DNA to complex **2***, the band due to intraligand transition at 339 nm exhibited hypochromism with a small red shift (7 nm). The results derived from the electronic absorption titration experiments suggested that the complexes (**1** and **2***) could bind to DNA through intercalation. However, **2*** interacted with CT DNA strongly, which might be due to the greater planar area of the complex, permitting it to penetrate and stack more intensely into DNA base pairs.⁴⁶ The K_b values of the complexes followed the order $1 < 2*$.

Ethidium Bromide (EB) Displacement by the Complexes. The binding of the Ru(η^6 -*p*-cymene) complexes with CT DNA could not be directly presented in the emission spectra, since the complexes were nonemissive in both the presence and absence of CT DNA. Hence, it has been studied by ethidium bromide (EB) displacement experiments. Usually EB emits fluorescence in the presence of DNA due to its strong intercalation between the adjacent DNA base pairs.⁴⁷ Hence, the EB displacement study can provide indirect evidence for the

Table 4. K_b , K_q and K_{app} Values for **1** and **2***

complex	K_b (M^{-1})	K_q (M^{-1})	K_{app} (M^{-1})
1	2.47×10^5	9.43×10^4	4.71×10^6
2*	3.73×10^5	1.29×10^5	6.37×10^6

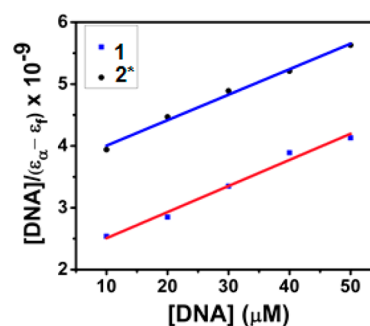


Figure 9. Plot of $[\text{DNA}]/(\epsilon_\alpha - \epsilon_t)$ versus $[\text{DNA}]$ for the titration of the complexes with CT DNA.

mode of binding. The displacement method is based on the decrease of fluorescence resulting from the displacement of EB from a DNA sequence by a quencher. The emission spectra of the DNA/EB (1/1) system with increasing concentration of the complexes (0–50 μM) are shown in Figure 10. From the observed decrease in the fluorescence intensity, it was inferred that the EB molecules were replaced by the complexes under investigation.⁴⁸ The binding propensity of the complexes with CT DNA was determined by the Stern–Volmer equation, $F^0/F = 1 + K_q[Q]$, where F^0 and F are the fluorescence intensities in the absence and presence of a complex, respectively. K_q is the linear Stern–Volmer quenching constant, and $[Q]$ is the concentration of the compound. The K_q values are obtained as

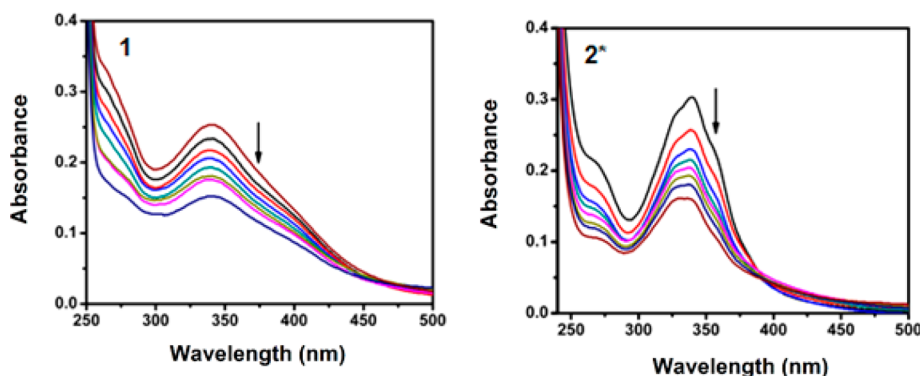


Figure 8. Absorption spectra of **1** and **2*** in Tris-HCl buffer upon addition of CT DNA. Conditions: $[\text{complex}] = 15 \mu\text{M}$, $[\text{DNA}] = 0\text{--}35 \mu\text{M}$. The arrow shows that the absorption intensity decreases upon increasing CT DNA concentration.

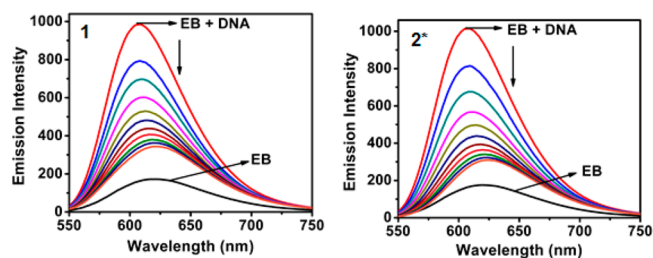


Figure 10. Fluorescence quenching curves of EB bound to DNA in the presence of **1** and **2***. Conditions: [DNA] = 5 μM , [EB] = 5 μM , [complex] = 0–50 μM .

a slope from the plot of F^0/F versus [Q] (Figure 11 and Table 4). Further, the apparent DNA binding constant (K_{app}) values

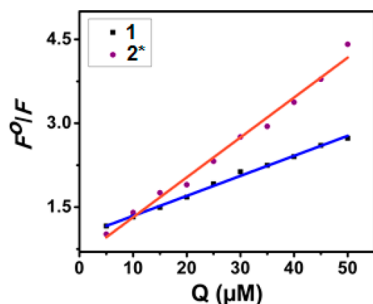


Figure 11. Stern–Volmer plots of fluorescence titrations of the complexes with CT DNA.

were calculated using the equation $K_{\text{EB}} [\text{EB}] = K_{\text{app}} [\text{complex}]$, where the complex concentration is the value at a 50% reduction in the fluorescence intensity of EB, K_{EB} ($1.0 \times 10^7 \text{ M}^{-1}$) is the DNA binding constant of EB, and [EB] is the concentration of EB (5 μM). It was clear from the data that complex **2*** bound more strongly with DNA than complex **1**, which was in agreement with the trend observed from the UV–vis absorption spectra. Moreover, the quenching and binding constant values of the complexes suggested that the interaction of complexes **1** and **2*** with CT DNA should be that of intercalation.⁴⁹

Changes in the Viscosity of CT DNA. To confirm the nature of the interaction between the complexes and CT DNA, viscosity measurements have been carried out. Accordingly, the increase in viscosity due to elongation of the double helix by the intercalating agents indicates an intercalative mode of binding. In contrast, a decrease/no change in viscosity due to bending of DNA base pairs or kinking of DNA helix substantiates groove binding.^{50,51} Viscosity values of CT DNA (100 μM) in the presence of increasing concentration (0–50 μM) of complexes **1** and **2*** are depicted in Figure 12. The increase in the viscosity of CT DNA with increase in concentration of the complexes confirmed an intercalative mode of binding.⁵⁰

Perturbation of Bands in the CD Spectra. The conformational changes in the environment of the nucleic acids induced by a complex can be studied by recording circular dichroism (CD) spectra.⁵² CT DNA showed positive and negative bands in its CD spectrum at 278 and 244 nm, respectively, due to base stacking and helicity of B-DNA.⁵³ Groove binding and electrostatically interacting complexes lead to less or no perturbation on the base stacking and helicity bands, whereas intercalating complexes enhance the intensity of both bands.⁵⁴

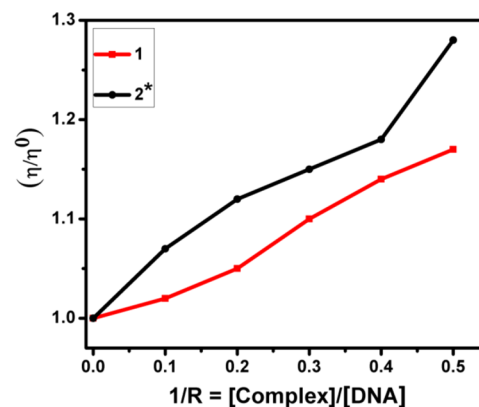


Figure 12. Effect of the complexes on the viscosity of CT DNA.

The CD spectrum of CT DNA (20 μM) after addition of complexes **1** and **2*** (5 μM) showed an increase in positive and a decrease in negative ellipticity with a small red shift, probably due to the unwinding of the DNA helix upon interaction with the complexes, and then transformed into A-DNA, which validated the intercalative binding mode of the complexes (Figure 13).^{55,56}

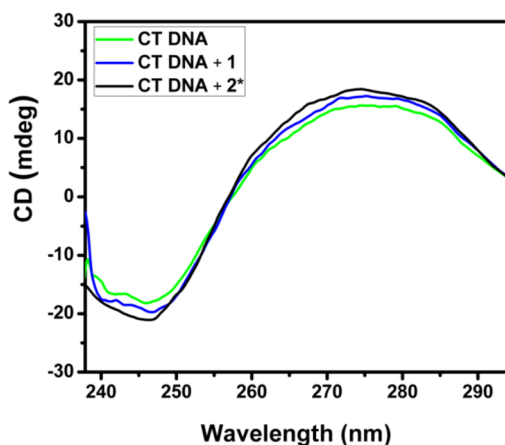


Figure 13. CD spectra of CT DNA in the absence and presence of the complexes in Tris-HCl buffer (pH 7.2) at room temperature. Conditions: [complex] = 5 μM , [DNA] = 20 μM .

DNA Cleavage by the Complexes. DNA is one of the most important cellular targets for complexes to exhibit good anticancer activity.^{57,58} The supercoiled (SC) pUC19/pBR322 DNA (40 μM) was incubated at 37 $^{\circ}\text{C}$ with complexes **1** (100 μM) and **2*** (50/100 μM) in a 5% DMF/5 mM Tris-HCl/50 mM NaCl buffer at pH 7.2 for 3 h. The cleaving efficiency of the complexes was assessed by their ability to convert SC DNA (Form I) into nicked circular (NC) DNA (Form II), while no linear DNA (Form III) was observed (Figures 14 and 15). The DNA cleavage efficiency followed the order **2*** (99.3%) > **1** (93.6%) in pUC19 and **2*** (99.8%) > **1** (54.7%) in pBR322 DNA, which reflected the fact that DNA cleavage by the complexes was in line with their DNA binding ability.

Interaction with BSA. *Fluorescence Quenching of BSA by the Complexes.* BSA protein shows fluorescence due to the presence of tyrosine and tryptophan residues.⁵⁹ To investigate the interaction between BSA and complexes **1** and **2***, fluorescence titration has been followed. The fluorescence spectra were recorded in the range of 290–500 nm (λ_{ex} 280

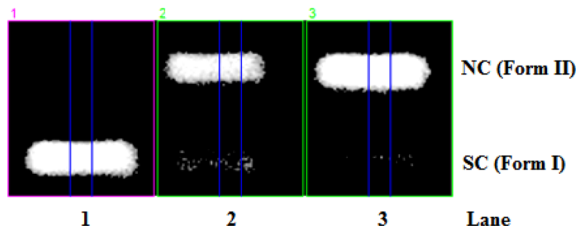


Figure 14. Cleavage of supercoiled pUC19 DNA ($40 \mu\text{M}$) by complexes **1** and **2*** in a buffer containing 5% DMF/5 mM Tris-HCl/50 mM NaCl (pH 7.2) at 37°C with an incubation time of 4 h: lane 1, DNA control; lane 2, DNA + **1** ($100 \mu\text{M}$); lane 3, DNA + **2*** ($50 \mu\text{M}$). Forms SC and NC are supercoiled and nicked circular DNA, respectively.

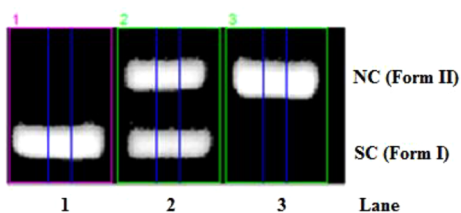


Figure 15. Cleavage of supercoiled pBR322 DNA ($40 \mu\text{M}$) by complexes **1** and **2*** in a buffer containing 5% DMF/5 mM Tris-HCl/50 mM NaCl (pH 7.2) at 37°C with an incubation time of 4 h: lane 1, DNA control; lane 2, DNA + **1** ($100 \mu\text{M}$); lane 3, DNA + **2*** ($100 \mu\text{M}$). Forms SC and NC are supercoiled and nicked circular DNA, respectively.

nm). The changes observed on the fluorescence spectra of BSA ($1 \mu\text{M}$) by the addition of increasing concentration of the complexes (0 – $20 \mu\text{M}$) are shown in Figure 16. The fluorescence intensity of BSA at 345 nm was quenched with a hypsochromic shift by the addition of complexes **1** (89%, 10 nm) and **2*** (82%, 8 nm). The red shift was due to the fact that the active sites in the protein were buried in a hydrophobic environment. The results showed the interaction between the Ru(η^6 -*p*-cymene) complexes and BSA.^{60,61} The fluorescence quenching constant (K_q) values were calculated from Stern–Volmer equation using an F^0/F versus $[Q]$ plot (Figure 17). When small molecules bind independently to a set of equivalent sites on a macromolecule, the equilibrium between free and bound molecules is represented by the Scatchard equation $\log[(F^0 - F)/F] = \log K_b + n \log [Q]$, where K_b is the binding constant of a complex with BSA and n is the number of binding sites. From the plot of $\log[(F^0 - F)/F]$ versus $\log [Q]$ (Figure 18), the number of binding sites (n) (0.924 (**1**) and 0.971 (**2***)) and binding constant (K_b) values have been obtained. The calculated K_q , K_b , and n values for the interaction

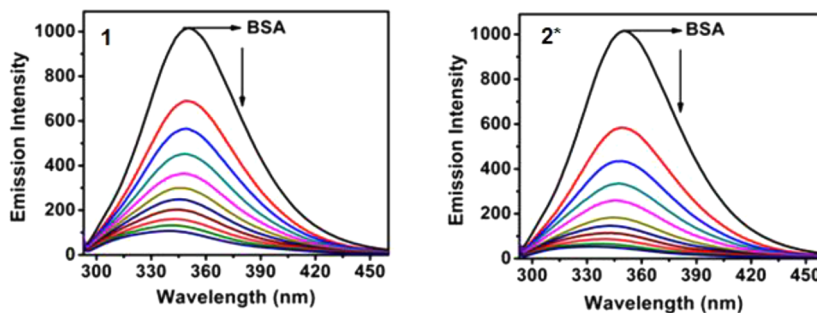


Figure 16. Fluorescence quenching curves of BSA in the absence and presence of **1** and **2***. Conditions: $[\text{BSA}] = 1 \mu\text{M}$, $[\text{complex}] = 0$ – $20 \mu\text{M}$.

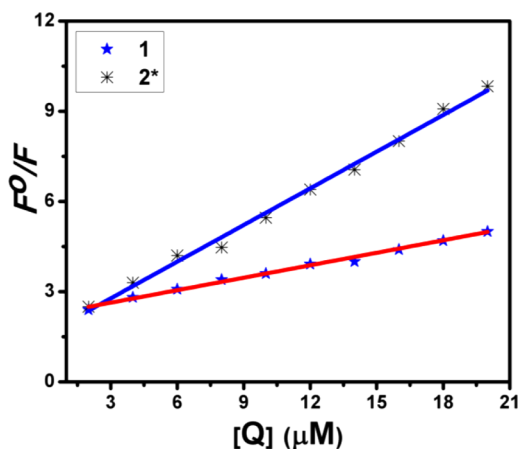


Figure 17. Stern–Volmer plots of the fluorescence titrations of the complexes with BSA.

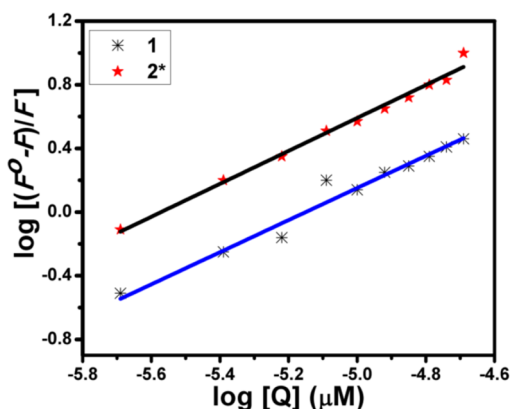


Figure 18. Scatchard plots of the fluorescence titrations of the complexes with BSA.

of complexes **1** and **2*** with BSA are gathered in Table 5. The estimated value of n was around 1 for complexes **1** and **2***. The

Table 5. K_b , K_q , and n Values for **1** and **2***

complex	K_b (M^{-1})	K_q (M^{-1})	n
1	2.42×10^7	4.17×10^5	0.924
2*	5.01×10^7	7.09×10^5	0.971

values of K_q and K_b suggested that the complexes strongly interacted with BSA and the binuclear complex (**2***) exhibited better interaction with BSA in comparison to **1**.

Mechanism of Quenching. The quenching of fluorescence intensity usually occurs by either dynamic or static mode. The mode of quenching was determined from electronic absorption spectra of BSA with and without the complexes (Figure 19).^{63,64} The absorption intensity of BSA (10 μM) gradually

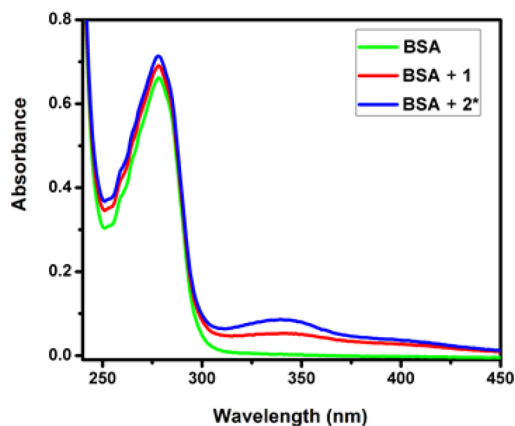


Figure 19. Absorption spectra of BSA (10 μM) and BSA with **1** and **2*** (4 μM).

increased without any shift in the position of the absorption band at 280 nm with the addition of the complexes (4 μM), which suggested static quenching.⁶⁵

Structural Changes in BSA. In synchronous fluorescence spectroscopy, the difference between excitation and emission wavelengths reflects the spectra of a different nature of chromophore.⁶⁶ With a small $\Delta\lambda$ value such as 15 nm, the synchronous fluorescence of BSA is characteristic of the tyrosine residue (Figure 20) and a large $\Delta\lambda$ value such as 60 nm is characteristic of the tryptophan residue (Figure 21).⁶⁷ When the concentration of complexes **1** and **2*** was increased (0–20 μM), the fluorescence intensity of the tyrosine residue at 304 nm decreased by 72.1 and 75.9% for complexes **1** and **2***, respectively. The tryptophan fluorescence emission showed significant decrease in the intensity (at 340 nm) (89.7 (**1**) and 84.2% (**2***)) without any shift in the position of the emission band. The results indicated that the complexes affected the microenvironments of both the tyrosine and tryptophan during the binding process, while the effect was more pronounced toward the tryptophan in comparison to tyrosine.⁶⁸

Anticancer Activity. Blood Compatibility. Assessing the hemolysis of drugs is crucial in evaluating their blood compatibility. Ru(η^6 -*p*-cymene) complexes with six different concentrations (25, 50, 75, 100, 250, and 500 $\mu\text{g/mL}$) were

tested for their toxicity against human red blood cells (RBC). The results were compared to the control cells treated with water, which produced 100% lysis. The complexes exhibited negligible red hemoglobin release, implying that they were negligibly toxic (Figure S24), which suggested that the Ru(η^6 -*p*-cymene) complexes (**1** and **2***) can be used for pharmacological actions.⁶⁹

Activity Against A549 and HepG-2. The positive results obtained from the DNA/protein interaction and antihemolytic studies for complexes **1** and **2*** have encouraged us to test their anticancer properties against cancer (lung (A549) and liver carcinoma (HepG-2)) and normal (mouse embryonic fibroblasts (L929)) cells. The IC_{50} values (50% inhibition of cell growth for 24 h) of the free ligands and the Ru(η^6 -*p*-cymene) complexes obtained from MTT assays are summarized in Table S4, and the percent cell death versus concentration is graphically presented in Figures 22 and 23. Media (DMSO/buffer) and cisplatin were used as controls under identical experimental conditions. The IC_{50} values for the free ligands were >140 μM against A549 and HepG-2 cell lines. Though complexes **1** (IC_{50} = 49.3 μM (A549), 62.7 μM (HepG-2)) and **2*** (IC_{50} = 11.5 μM (A549), 35.3 μM (HepG-2)) were active against the cancer cells, the activity of **2*** was comparable with that of cisplatin (IC_{50} = 21.3 μM (A549), 21.5 μM (HepG-2)) at both low and high micromolar concentrations. The high activity of Ru(η^6 -*p*-cymene) complexes might have initiated from the strong interaction of the complexes with both DNA and protein. In addition, *in vitro* cytotoxicity studies of the free ligands and the Ru(η^6 -*p*-cymene) complexes against L929 mouse embryonic fibroblasts (normal cells) have been carried out (Figure S25). The IC_{50} values of the free ligands and Ru(η^6 -*p*-cymene) complexes have been found to be above 500 and 800 μM , respectively (cisplatin IC_{50} = 6.0 (L929)), which confirmed that the Ru(η^6 -*p*-cymene) complexes were specifically active on cancer cells.

Mode of Cell Death. The mode of cell death was visualized using a fluorescent staining method. A549 cells treated with the IC_{50} concentration of complex **2*** (IC_{50} = 11.5 μM) were subjected to confocal microscopic studies. In this study, 4',6-diamidino-2-phenylindole (DAPI, blue), fluorescein isothiocyanate (FITC, green), and propidium iodide fluorescence (PI, red) stains were used to assess the morphological changes in the cell after treatment with **2***. DAPI binds strongly to A-T rich regions in DNA and passes through an intact cell membrane. FITC acts as a phosphatidyl serine tracer and suggests the presence of apoptosis. PI can only penetrate cells where the cell membrane has been compromised. The confocal microscopic images indicated substantial changes in the

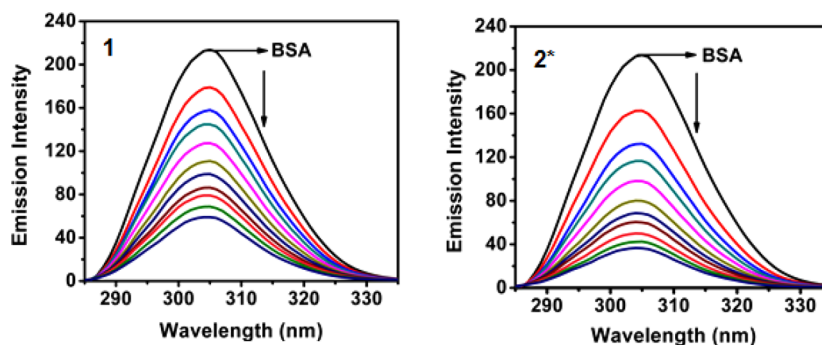


Figure 20. Synchronous spectra of BSA (1 μM) as a function of concentration of **1** and **2*** (0–20 μM), when $\Delta\lambda$ = 15 nm.

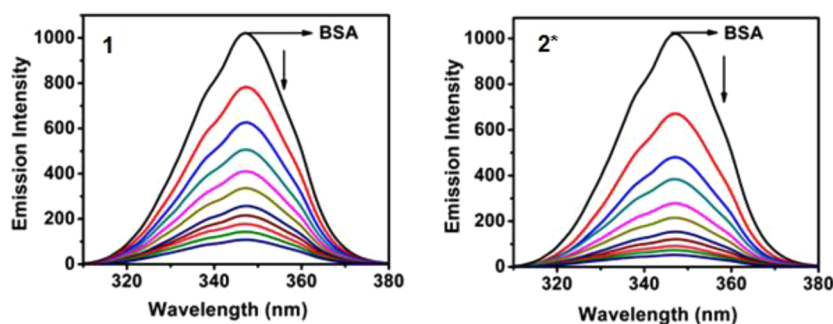


Figure 21. Synchronous spectra of BSA ($1 \mu\text{M}$) as a function of concentration of **1** and **2*** ($0\text{--}20 \mu\text{M}$), when $\Delta\lambda = 60 \text{ nm}$.

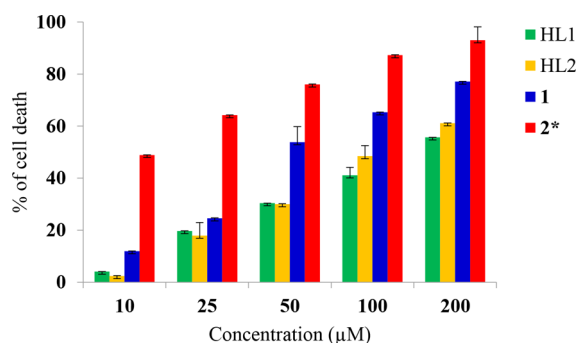


Figure 22. Comparison of anticancer activity of the ligands (HL1 and HL2) and complexes (**1** and **2***) against A549 cancer cells. Data are mean \pm SD of three independent experiments with each experiment conducted in triplicate.

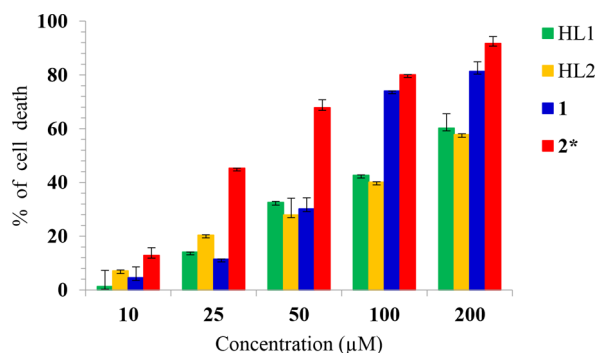


Figure 23. Comparison of anticancer activity of the ligands (HL1 and HL2) and complexes (**1** and **2***) against HepG-2 cancer cells. Data are mean \pm SD of three independent experiments with each experiment conducted in triplicate.

morphology of the cells after treatment with **2***, which suggested an apoptosis mechanism for cell death (Figure 24).⁷⁰

DNA fragmentation was confirmed by agarose gel (2%) electrophoresis. A549 cells treated with two different concentrations (11.5 and 23 μM) of complex **2*** were incubated for 24 h. DNA was extracted from untreated and treated cells, and its fragmentation was visualized.⁷¹ Interestingly, after the treatment with **2***, DNA underwent concentration-dependent fragmentation (Figure 25), which clearly indicated that the cell death mechanism was apoptosis.

CONCLUSIONS

Mono- and binuclear $\text{Ru}(\eta^6\text{-}p\text{-cymene})$ complexes with TSC ligands were exclusively formed in different reactions and characterized. The TSC ligands coordinated to $\text{Ru}(\text{II})$ ion

through imine nitrogen and sulfur/thiolato sulfur. Geometries of both the formed and expected monomers (**1** and **2**) and dimers (**1*** and **2***) were optimized and compared. Free energies revealed that dimerization in both cases was endergonic but the process was less endergonic in complex **2**, making dimerization slightly easier, in agreement with experiment. The methyl group present on the terminal nitrogen atom in complex **2** enhanced the electron density on the sulfur atom, which enabled the sulfur atom to easily coordinate with another Ru, thus favoring the dimerization of complex **2**. Another factor that enabled the dimerization was the C–S bond order in complex **2**. The lower double-bond character made it easier to cleave and form the new S–Ru2 bond. The effect of other substituents will be evaluated in the future. The DNA interaction property of complexes **1** and **2*** evaluated by electronic, emission, viscosity, and CD measurements supported the fact that the complexes could bind to DNA via intercalation in the order $2^* > 1$. The complexes also efficiently cleaved the pUC19 and pBR322 plasmid DNA. In addition, the BSA protein binding affinity of the $\text{Ru}(\eta^6\text{-}p\text{-cymene})$ complexes, investigated by absorption and emission spectroscopy techniques, suggested that **2*** had a stronger binding capacity in comparison to **1**. The hemolysis results showed that the complexes could be used for drug tests, as they did not show any toxicity against RBC. The complexes showed significant activity against cancer cells (A549 and HepG-2) through apoptosis without harming normal cells (L929). Complex **2*** had a better activity than **1** presumably due to its higher DNA/protein binding affinity. Moreover, **2*** ($\text{IC}_{50} = 11.5 \mu\text{M}$) showed superior activity in comparison to even cisplatin ($\text{IC}_{50} = 21.3 \mu\text{M}$) in the A549 cell line. The morphological changes in A549 cells evaluated by immunofluorescence and DNA fragmentation studies clearly suggested that the cell death was apoptosis. *In vivo* studies will be carried out in the future to realize its application.

EXPERIMENTAL SECTION

General Methods. The required chemicals, biomolecules, and solvents were purchased from commercial suppliers (Sigma-Aldrich, Promega, Biologend, BD Biosciences, and Alfa Aesar). $[\text{RuCl}_2(p\text{-cymene})_2]$ and TSC ligands were synthesized by following the previously reported methods.^{28,72} DNA and protein binding experiments, hemolysis assay, 3-[4,5-dimethylthiazol-2-yl]-2,5-diphenyltetrazolium bromide (MTT) assay,^{28,73,74} fluorescent staining, and DNA fragmentation were carried out for the compounds according to the literature procedures.⁷⁵

(E)-2-((1*H*-Indol-3-yl)methylene)hydrazinecarbothioamide (HL1). Thiosemicarbazide (0.91 g, 10 mmol) and indole-3-carboxaldehyde (1.45 g, 10 mmol) were used. Yield: 91%. Color: white. Mp: 162 °C. Anal. Calcd for $\text{C}_{10}\text{H}_{10}\text{N}_4\text{S}$: C, 55.02; H, 4.62; N, 25.67; S, 14.69. Found: C, 55.24; H, 4.78; N, 25.51; S, 14.76. UV–vis

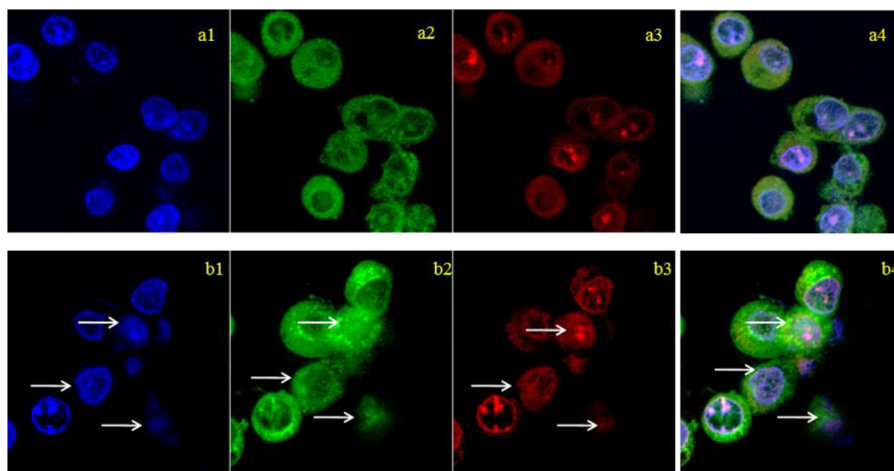


Figure 24. DAPI (blue), FITC (green), and PI (red) fluorescence staining for the detection of apoptosis in A549 cells. Cells were treated with **2*** ($11.5 \mu\text{M}$). The fluorescence signals of DAPI, FITC, and PI were examined under a confocal laser scanning microscope. Legend: control (a1-DAPI, a2-FITC, a3-PI, and a4-merged) and treatment with **2*** (b1-DAPI, b2-FITC, b3-PI, and b4-merged). Arrows indicate apoptotic cancer cells.

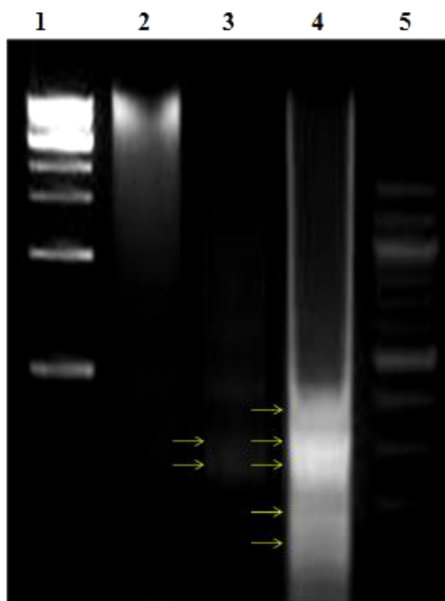


Figure 25. DNA (A549) fragmentation by **2***: lane 1, 1 kb DNA ladder; lane 2, control; lane 3, **2*** ($11.5 \mu\text{M}$); lane 4, **2*** ($23.0 \mu\text{M}$); lane 5, 100 bp DNA ladder. Arrows indicate the DNA fragmentation in comparison to control.

(CH_3OH): λ_{max} (nm) 264, 330. FT-IR (KBr): ν (cm^{-1}) 3448, 3312 (N-H), 3230 (H-N-C=S), 1548 (C=N), 1295 (C=S). ^1H NMR (500 MHz, $\text{DMSO}-d_6$): δ (ppm) 7.12 (ddd, $J = 7.9, 7.1, 1.1$ Hz, 1H, H7), 7.19 (ddd, $J = 8.1, 7.1, 1.2$ Hz, 1H, H6), 7.40 (bs, 1H, $\text{NH}(\text{NH}_2)$), 7.42 (dt, $J = 8.1, 1.0$ Hz, 1H, H5), 7.81 (d, $J = 2.8$ Hz, 1H, H3), 8.00 (bs, 1H, $\text{NH}(\text{NH}_2)$), 8.21 (d, $J = 7.9$ Hz, 1H, H8), 8.29 (s, 1H, H1), 11.16 (s, 1H, N-NH-CS), 11.59 (bs, 1H, indole NH). ^{13}C NMR (125.80 MHz, $\text{DMSO}-d_6$): δ (ppm) 111.10 (C2), 111.72 (C5), 120.58 (C7), 122.09 (C8), 122.59 (C6), 123.95 (C9), 130.92 (C3), 137.02 (C4), 141.78 (C1), 176.51 (C10). HR-ESI-MS: m/z found (calcd) 219.0713 (219.0704) $\{[\text{M} + \text{H}^+]^+ = [\text{C}_{10}\text{H}_{11}\text{N}_4\text{S}]^+\}$.

(E)-2-((1H-Indol-3-yl)methylene)-N-methylhydrazinecarbothioamide (HL2). 4-Methylthiosemicarbazide (1.05 g, 10 mmol) and indole-3-carboxaldehyde (1.45 g, 10 mmol) were used. Yield: 85%. Color: white. Mp: 154°C . Anal. Calcd for $\text{C}_{11}\text{H}_{12}\text{N}_4\text{S}$: C, 56.87; H, 5.21; N, 24.12; S, 13.80. Found: C, 56.94; H, 5.32; N, 24.0; S, 13.91. UV-vis (CH_3OH): λ_{max} (nm) 262, 329. FT-IR (KBr): ν (cm^{-1}) 3440, 3325 (N-H), 3238 (H-N-C=S), 1551 (C=N), 1299 (C=S). ^1H

NMR (500 MHz, $\text{DMSO}-d_6$): δ (ppm) 3.08 (d, $J = 4.7$ Hz, 3H, $\text{NH}-\text{CH}_3$), 7.13 (ddd, $J = 7.9, 7.1, 1.1$ Hz, 1H, H7), 7.20 (ddd, $J = 8.1, 6.9, 1.3$ Hz, 1H, H6), 7.42 (dt, $J = 8.1, 1.0$ Hz, 1H, H5), 7.89 (d, $J = 2.7$ Hz, 1H, H3), 7.90 (q, $J = 4.7$ Hz, 1H, $\text{NH}-\text{CH}_3$), 8.27 (d, $J = 7.8$ Hz, 1H, H8), 8.31 (s, 1H, H1), 11.16 (s, 1H, N-NH-CS), 11.59 (bs, 1H, indole NH). ^{13}C NMR (125 MHz, $\text{DMSO}-d_6$): δ (ppm) 30.99 ($\text{NH}-\text{CH}_3$), 111.17 (C5), 111.69 (C2), 120.49 (C7), 122.18 (C8), 122.59 (C6), 123.93 (C9), 130.75 (C3), 137.01 (C4), 140.43 (C1), 176.77 (C10). HR-ESI-MS: m/z found (calcd) 233.0862 (233.0861) $\{[\text{M} + \text{H}^+]^+ = [\text{C}_{11}\text{H}_{13}\text{N}_4\text{S}]^+\}$.

Synthesis of the $\text{Ru}(\eta^6\text{-}p\text{-Cymene})$ Complexes. TSC ligand (2 mmol) and $[\text{RuCl}_2(p\text{-cymene})]_2$ (1 mmol) were dissolved in 25 mL of toluene, and the resultant solution was stirred for 1 h at $25\text{--}27^\circ\text{C}$ to form an orange solid.⁷⁶ The precipitate was filtered, washed with toluene and hexane, and dried *in vacuo*. The pure complexes were obtained by recrystallization from methanol solution.

$[\text{Ru}(\eta^6\text{-}p\text{-cymene})\text{Cl}]\text{Cl}$ (**1**). HL1 (436 mg, 2 mmol) and $[\text{RuCl}_2(p\text{-cymene})]_2$ (612 mg, 1 mmol) were used. Yield: 91%. Color: orange. Mp: 217°C . Anal. Calcd for $\text{C}_{20}\text{H}_{24}\text{Cl}_2\text{N}_4\text{RuS}$: C, 45.80; H, 4.61; N, 10.68; S, 6.11. Found: C, 45.93; H, 4.76; N, 10.47; S, 6.30. UV-vis (CH_3OH): λ_{max} (nm) 267, 342, 432. FT-IR (KBr): ν (cm^{-1}) 3452, 3315 (N-H), 3219 (H-N-C=S), 1501 (C=N), 1244 (C=S). ^1H NMR (500 MHz, $\text{CD}_3\text{OD}-d_4$): δ (ppm) 1.05 (d, $J = 6.9$ Hz, 3H, H12), 1.13 (d, $J = 6.9$ Hz, 3H, H11), 2.03 (s, 3H, H20), 2.59 (spt, $J = 6.8$ Hz, 1H, H13), 5.18 (dd, $J = 6.0, 1.1$ Hz, 1H, H15), 5.27 (dd, $J = 6.0, 1.0$ Hz, 1H, H16), 5.32 (dd, $J = 6.0, 1.0$ Hz, 1H, H18), 5.71 (dd, $J = 6.0, 1.1$ Hz, 1H, H17), 7.20 (ddd, $J = 8.0, 7.1, 1.0$ Hz, 1H, H7), 7.25 (ddd, $J = 8.2, 6.9, 1.3$ Hz, 1H, H6), 7.50 (dt, $J = 7.9, 1.0$ Hz, 1H, H5), 7.69 (dt, $J = 7.8, 1.0$ Hz, 1H, H8), 8.79 (s, 1H, H3), 9.01 (s, 1H, H1), 11.83 (s, 1H, indole NH). ^{13}C NMR (125 MHz, $\text{CD}_3\text{OD}-d_4$): δ (ppm) 18.85 (C20), 21.79 (C12), 23.15 (C11), 32.23 (C13), 84.37 (C15), 85.65 (C18), 89.58 (C17), 89.76 (C16), 104.38 (C19), 104.55 (C14), 110.10 (C2), 114.02 (C5), 118.61 (C8), 123.36 (C7), 125.01 (C6), 128.85 (C9), 132.63 (C3), 138.05 (C4), 156.91 (C1), 179.08 (C10). ^{13}C DEPT 135 NMR (125 MHz, $\text{CD}_3\text{OD}-d_4$): δ : ppm 18.85 (C20), 21.78 (C12), 23.16 (C11), 32.24 (C13), 84.38 (C15), 85.64 (C18), 89.59 (C17), 89.76 (C16), 114.02 (C5), 118.62 (C8), 123.37 (C7), 125.00 (C6), 132.62 (C3), 156.90 (C1). HR-ESI-MS: m/z found (calcd) 453.0685 (453.0687) $\{[\text{M} - \text{H}^+ - 2\text{Cl}^-]^+ = [\text{C}_{20}\text{H}_{23}\text{N}_4\text{RuS}]^+\}$.

$[\text{Ru}(\eta^6\text{-}p\text{-cymene})(\text{L2})]_2\text{Cl}_2$ (**2***). HL2 (464 mg, 2 mmol) and $[\text{RuCl}_2(p\text{-cymene})]_2$ (612 mg, 1 mmol) were used. Yield: 83%. Color: orange. Mp: 206°C . Anal. Calcd for $\text{C}_{42}\text{H}_{50}\text{Cl}_2\text{N}_8\text{Ru}_2\text{S}_2$: C, 50.24; H, 5.02; N, 11.16; S, 6.39. Found: C, 50.17; H, 5.13; N, 11.00; S, 6.51. UV-vis (CH_3OH): λ_{max} (nm) 271, 339, 429. FT-IR (KBr): ν (cm^{-1}) 3435, 3321 (N-H), 1503 (C=N), 1230 (C=S). ^1H NMR (500 MHz, $\text{CD}_3\text{OD}-d_4$): δ (ppm) 1.05 (d, $J = 6.9$ Hz, 6H, H12), 1.12 (d, J

= 6.9 Hz, 6H, H11), 2.02 (s, 6H, H20), 2.59 (spt, $J = 6.8$ Hz, 2H, H13), 3.01 (bs, 6H, NH-CH₃), 5.21 (dd, $J = 6.0, 1.0$ Hz, 2H, H15), 5.26–5.27 (m, 2H, H16), 5.35 (dd, $J = 6.0, 0.9$ Hz, 2H, H18), 5.72 (dd, $J = 6.0, 1.0$ Hz, 2H, H17), 7.17–7.22 (m, 2H, H7), 7.22–7.27 (m, 2H, H6), 7.49 (d, $J = 8.2$ Hz, 2H, H5), 7.69 (d, $J = 7.6$ Hz, 2H, H8), 8.80 (s, 2H, H3), 9.00 (s, 2H, H1), 11.80 (s, 2H, indole NH). ¹³C NMR (125 MHz, CD₃OD-*d*₄): δ (ppm) 18.84 (C20), 21.77 (C12), 23.20 (C11), 32.22 (C13), 32.37 (CH₃NH), 84.87 (C15), 85.76 (C18), 89.47 (C17), 89.83 (C16), 104.27 (C19), 104.67 (C14), 110.13 (C2), 114.00 (C5), 118.61 (C8), 123.34 (C7), 124.98 (C6), 128.87 (C9), 132.51 (C3), 138.01 (C4), 155.05 (C1), 176.76 (C10). ¹³C DEPT 135 NMR (125 MHz, CD₃OD-*d*₄): δ (ppm) 18.84 (C20), 21.76 (C12), 23.24 (C11), 32.21 (C13), 32.38 (NH-CH₃), 84.87 (C15), 85.73 (C18), 89.44 (C17), 89.84 (C16), 113.99 (C5), 118.60 (C8), 123.35 (C7), 124.96 (C6), 132.47 (C3), 155.05 (C1). HR-ESI-MS: m/z found (calcd) 467.0191 (467.0843) {[M - 2Cl]²⁺ = [C₄₂H₅₀N₈Ru₂S₂]²⁺}.

Computational Details. The initial coordinates of complexes **1** and **2*** were obtained directly from the X-ray crystal structures, while **1*** and **2** were modeled. The ground state geometries of **1**, **2**, **1***, and **2*** were fully optimized by density functional theory (DFT) with the B3LYP⁷⁷ functional and SDD basis set for Ru/6-311g(d,p) for other atoms. Geometry optimizations were performed without any symmetry constraints with methanol as solvent using the polarizable continuum model (PCM).⁷⁸ The optimized structures were confirmed to be local minima through harmonic analysis. ΔG values were calculated at the same level of approximation for $T = 298.15$ K and $P = 1.0$ atm. All calculations were performed using Gaussian 09 (G09).⁷⁹

■ ASSOCIATED CONTENT

● Supporting Information

The Supporting Information is available free of charge on the ACS Publications website at DOI: 10.1021/acs.organomet.8b00004.

Details of physical measurements, 1D/2D NMR spectra of the compounds, and toxicity data (PDF)

Accession Codes

CCDC 1581131–1581134 contain the supplementary crystallographic data for this paper. These data can be obtained free of charge via www.ccdc.cam.ac.uk/data_request/cif, or by emailing data_request@ccdc.cam.ac.uk, or by contacting The Cambridge Crystallographic Data Centre, 12 Union Road, Cambridge CB2 1EZ, UK; fax: +44 1223 336033.

■ AUTHOR INFORMATION

Corresponding Author

*E-mail for R.K.: kar@nitt.edu.

ORCID

Manoharan Muthu Tamizh: 0000-0002-0673-5177

Ramasamy Karvembu: 0000-0001-8966-8602

Notes

The authors declare no competing financial interest.

■ ACKNOWLEDGMENTS

J.H. thanks the University Grants Commission for a fellowship (F1-17.1/2012-13/RGNF-2012-13-ST-AND-18716). P.V. thanks the Council of Scientific and Industrial Research for the award of an Emeritus Scientistship (No. 21(0936)/12/EMR-II), Department of Science and Technology (DST) of India, for a Major Research Project (SB/S1/PC-52/2012) and the DST-PURSE HPC facility (SR/FT/LS-113/2009) of Bharathidasan University.

■ REFERENCES

- Arnesano, F.; Losacco, M.; Natile, G. An updated view of cisplatin transport. *Eur. J. Inorg. Chem.* **2013**, *2013*, 2701–2711.
- Hoeschele, J. D. In remembrance of Barnett Rosenberg. *Dalton Trans.* **2009**, 10648–10650.
- Reedijk, J. Platinum anticancer coordination compounds: Study of DNA binding inspires new drug design. *Eur. J. Inorg. Chem.* **2009**, 2009, 1303–1312.
- Boulikas, T.; Vougiouka, M. Cisplatin and platinum drugs at the molecular level. *Oncol. Rep.* **2003**, *10*, 1663–1682.
- Wong, E.; Giandomenico, C. M. Current status of platinum based antitumor drugs. *Chem. Rev.* **1999**, *99*, 2451–2466.
- Galanski, M.; Arion, V. B.; Jakupec, M. A.; Keppler, B. K. Recent developments in the field of tumor inhibiting metal complexes. *Curr. Pharm. Des.* **2003**, *9*, 2078–2089.
- Wang, D.; Lippard, S. J. Cellular processing of platinum anticancer drugs. *Nat. Rev. Drug Discovery* **2005**, *4*, 307–320.
- Siu, P. K. M.; Ma, D. L.; Che, C. M. Luminescent cyclometalated platinum(II) complexes with amino acid ligands for protein binding. *Chem. Commun.* **2005**, 1025–1027.
- Grozav, A.; Gaina, L. I.; Pileczki, V.; Crisan, O.; Dumitrescu, L. S.; Therrien, B.; Zaharia, V.; Neagoe, I. B. The synthesis and antiproliferative activities of new arylidene hydrazinyl thiazole derivatives. *Int. J. Mol. Sci.* **2014**, *15*, 22059–22072.
- Bosl, G. J.; Motzer, R. J. Testicular germ cell cancer. *N. Engl. J. Med.* **1997**, *337*, 242–253.
- Reedijk, J. Medicinal applications of metal complexes binding to biological macromolecules. *Macromol. Symp.* **2008**, *270*, 193–201.
- Fricker, S. P. Metal based drugs: From serendipity to design. *Dalton Trans.* **2007**, 4903–4917.
- Clarke, M. J. Ruthenium metallopharmaceuticals. *Coord. Chem. Rev.* **2003**, *236*, 209–233.
- Bratsos, I.; Jedner, S.; Gianferrara, T.; Alessio, E. Ruthenium anticancer compounds: Challenges and expectations. *Chimia* **2007**, *61*, 692–697.
- Rademaker-Lakhai, J. M.; Van Den Bongard, D.; Plum, D.; Beijnen, J. H.; Schellens, J. H. M. A phase I and pharmacological study with imidazolium-*trans*-DMSO-imidazole-tetrachlororuthenate, a novel ruthenium anticancer agent. *Clin. Cancer Res.* **2004**, *10*, 3717–3727.
- Lentz, F.; Drescher, A.; Lindauer, A.; Henke, M.; Hilger, R. A.; Hartinger, C. G.; Scheulen, M. E.; Dittrich, C.; Keppler, B. K.; Jaehde, U. Pharmacokinetics of a novel anticancer ruthenium complex (KP1019, FFC14A) in a phase I dose escalation study. *Anti-Cancer Drugs* **2009**, *20*, 97–103.
- Gianferrara, T.; Bratsos, I.; Alessio, E. A categorization of metal anticancer compounds based on their mode of action. *Dalton Trans.* **2009**, 38, 7588–7598.
- Dale, L. D.; Tocher, J. H.; Dyson, T. M.; Edwards, D. I.; Tocher, D. A. Studies on DNA damage and induction of SOS repair by novel multifunctional bioreducible compounds. A metronidazole adduct of a ruthenium-arene compound. *Anti-Cancer Drug Des.* **1992**, *7*, 3–14.
- Chen, H. M.; Parkinson, J. A.; Parsons, S.; Coxall, R. A.; Gould, R. O.; Sadler, P. J. Highly selective binding of organometallic ruthenium ethylenediamine complexes to nucleic acids: Novel recognition mechanisms. *J. Am. Chem. Soc.* **2002**, *124*, 3064–3082.
- (a) Sclaro, C.; Bergamo, A.; Brescacin, L.; Delfino, M.; Cocchiotto, R.; Laurenczy, G.; Geldbach, T. J.; Sava, G.; Dyson, P. J. *In vitro* and *in vivo* evaluation of ruthenium(II)-arene PTA complexes. *J. Med. Chem.* **2005**, *48*, 4161–4171. (b) Bergamo, A.; Masi, A.; Dyson, P. J.; Sava, G. Modulation of the metastatic progression of breast cancer with an organometallic ruthenium compound. *Int. J. Oncol.* **2008**, *33*, 1281–1289. (c) Chatterjee, S.; Kundu, S.; Bhattacharyya, A.; Hertinger, C. G.; Dyson, P. J. The ruthenium(II)-arene compound RAPTA-C induces apoptosis in EAC cells through mitochondrial and p53-JNK pathways. *JBIC, J. Biol. Inorg. Chem.* **2008**, *13*, 1149–1155.
- (a) Allardyce, C. S.; Dyson, P. J.; Ellis, D. J.; Heath, S. L. [Ru(η^6 -p-cymene)Cl₂(pta)] (pta = 1,3,5-triaza-7-phosphatricyclo-[3.3.1.1]-decane): A water soluble compound that exhibits pH dependent

- DNA binding providing selectivity for diseased cells. *Chem. Commun.* **2001**, *15*, 1396–1397. (b) Ang, W. H.; Daldini, E.; Scolaro, C.; Scopelliti, R.; Jeanneret, L. J.; Dyson, P. J. Development of organometallic ruthenium-arene anticancer drugs that resist hydrolysis. *Inorg. Chem.* **2006**, *45*, 9006–9013. (c) Scolaro, C.; Geldbach, T. J.; Rochat, S.; Dorcier, A.; Gossens, C.; Bergamo, A.; Cocchietto, M.; Tavernelli, I.; Sava, G.; Rothlisberger, U.; Dyson, P. J. Influence of hydrogen bonding substituents on the cytotoxicity of RAPTA compounds. *Organometallics* **2006**, *25*, 756–765. (d) Ang, W. H.; Daldini, E.; Jeanneret, L. J.; Dyson, P. J. Strategy to tether organometallic ruthenium-arene anticancer compounds to recombinant human serum albumin. *Inorg. Chem.* **2007**, *46*, 9048–9050. (e) Vock, C. A.; Renfrew, A. K.; Scopelliti, R.; Jeanneret, L. J.; Dyson, P. J. Influence of the diketonato ligand on the cytotoxicities of $[\text{Ru}(\eta^6\text{-}p\text{-cymene})(\text{R}_2\text{acac})(\text{PTA})]^+$ complexes (PTA = 1, 3, 5-triaza-7-phosphaadamantane). *Eur. J. Inorg. Chem.* **2008**, 1661–1671. (f) Renfrew, A. K.; Phillips, A. D.; Tapaviscza, E.; Scopelliti, U.; Rothlisberger, U.; Dyson, P. J. Influence of structural variation on the anticancer activity of RAPTA type complexes: PTN versus PTA. *Organometallics* **2009**, *28*, S061–S071.
- (22) (a) Bruijninx, P. C. A.; Sadler, P. J. Controlling platinum, ruthenium and osmium reactivity for anticancer drug design. *Adv. Inorg. Chem.* **2009**, *61*, 1–62. (b) Singh, S. K.; Joshi, S.; Singh, A. R.; Saxena, J. K.; Pandey, D. S. DNA binding and topoisomerase II inhibitory activity of water soluble ruthenium(II) and rhodium(III) complexes. *Inorg. Chem.* **2007**, *46*, 10869–10876. (c) Peacock, A. F. A.; Sadler, P. J. Medicinal organometallic chemistry: Designing metal arene complexes as anticancer agents. *Chem. - Asian J.* **2008**, *3*, 1890–1899.
- (23) Yu, Y.; Kalinowski, D. S.; Kovacevic, Z.; Siafakas, A. R.; Jansson, P. J.; Stefani, C.; Lovejoy, D. B.; Sharpe, P. C.; Bernhardt, P. V.; Richardson, D. R. Thiosemicarbazones from the old to new: Iron chelators that are more than just ribonucleotide reductase inhibitors. *J. Med. Chem.* **2009**, *52*, S271–S294.
- (24) French, F. A.; Blanz, E. J. The carcinostatic activity of thiosemicarbazones of formyl heteroaromatic compounds. Primary correlation. *J. Med. Chem.* **1966**, *9*, S85–S89.
- (25) Adsule, S.; Barve, V.; Chen, D.; Ahmed, F.; Dou, Q. P.; Padhye, S.; Sarkar, F. H. Novel Schiff base copper complexes of quinoline-2-carboxaldehyde as proteasome inhibitors in human prostate cancer cells. *J. Med. Chem.* **2006**, *49*, 7242–7246.
- (26) Richardson, D. R.; Kalinowski, D. S.; Richardson, V.; Sharpe, P. C.; Lovejoy, D. B.; Islam, M.; Bernhardt, P. V. 2-Acetylpyridine thiosemicarbazones are potent iron chelators and antiproliferative agents: Redox activity, iron complexation and characterization of their antitumor activity. *J. Med. Chem.* **2009**, *52*, 1459–1470.
- (27) Alomar, K.; Landreau, A.; Kempf, M.; Khan, M. A.; Allain, M.; Bouet, G. Synthesis, crystal structure, characterization of zinc(II), cadmium(II) complexes with 3-thiophene aldehyde thiosemicarbazone (3TTSCH). Biological activities of 3TTSCH and its complexes. *J. Inorg. Biochem.* **2010**, *104*, 397–404.
- (28) Haribabu, J.; Jeyalakshmi, K.; Arun, Y.; Bhuvanesh, N. S. P.; Perumal, P. T.; Karvembu, R. Synthesis of Ni(II) complexes bearing indole based thiosemicarbazone ligands for interaction with biomolecules and some biological applications. *JBIC, J. Biol. Inorg. Chem.* **2017**, *22*, 461–480.
- (29) (a) Beckford, F.; Dourth, D.; Shalowski, M., Jr.; Didion, J.; Thessing, J.; Woods, J.; Crowell, V.; Gerasimchuk, N.; Gonzalez-Sarrias, A.; Seeram, N. P. Half-sandwich ruthenium-arene complexes with thiosemicarbazones: Synthesis and biological evaluation of $[(\eta^6\text{-}p\text{-cymene})\text{Ru}(\text{piperonal thiosemicarbazones})\text{Cl}]\text{Cl}$ complexes. *J. Inorg. Biochem.* **2011**, *105*, 1019–1029. (b) Beckford, F.; Thessing, J.; Woods, J.; Didion, J.; Gerasimchuk, N.; Gonzalez-Sarrias, A.; Seeram, N. P. Synthesis and structure of $[(\eta^6\text{-}p\text{-cymene})\text{Ru}(2\text{-anthracen-9-ylmethylene-N-ethylhydrazinecarbothioamide})\text{Cl}]\text{Cl}$; biological evaluation, topoisomerase II inhibition and reaction with DNA and human serum albumin. *Metallomics* **2011**, *3*, 491–502.
- (30) (a) Adams, M.; Li, Y.; Khot, H.; De Kock, C.; Smith, P. J.; Land, K.; Chibalea, K.; Smith, G. S. The synthesis and antiparasitic activity of aryl and ferrocenyl derived thiosemicarbazone ruthenium(II)-arene complexes. *Dalton Trans.* **2013**, *42*, 4677–4685. (b) Adams, M.; De Kock, C.; Smith, P. J.; Land, K. M.; Liu, N.; Hopper, M.; Hsiao, A.; Burgoyne, A. R.; Stringer, T.; Meyer, M.; Wiesner, L.; Chibalea, K.; Smith, G. S. Improved antiparasitic activity by incorporation of organosilane entities into half-sandwich ruthenium(II) and rhodium(III) thiosemicarbazone complexes. *Dalton Trans.* **2015**, *44*, 2456–2468.
- (31) (a) Su, W.; Qian, Q.; Li, P.; Lei, X.; Xiao, Q.; Huang, S.; Huang, C.; Cui, J. Synthesis, characterization, and anticancer activity of a series of ketone- N^+ -substituted thiosemicarbazones and their ruthenium(II)-arene complexes. *Inorg. Chem.* **2013**, *52*, 12440–12449. (b) Huang, S.; Peng, S.; Su, W.; Tang, Z.; Cui, J.; Huang, C.; Xiao, Q. *In vitro* interaction investigation between three Ru(II)-arene complexes and human serum albumin: Structural influences. *RSC Adv.* **2016**, *6*, 47043–47054. (c) Su, W.; Tang, Z.; Xiao, Q.; Li, P.; Qian, Q.; Lei, X.; Huang, S.; Peng, B.; Cui, J.; Huang, C. J. Synthesis, structures, antiproliferative activity of a series of ruthenium(II)-arene derivatives of thiosemicarbazones ligands. *J. Organomet. Chem.* **2015**, *783*, 10–16.
- (32) Raja, N.; Devika, N.; Gupta, G.; Nayak, V. L.; Kamal, A.; Nagesh, N.; Therrien, B. Biological activities of pyrenyl derived thiosemicarbazone half-sandwich complexes. *J. Organomet. Chem.* **2015**, *794*, 104–114.
- (33) Beckford, F. A.; Leblanc, G.; Thessing, J.; Shalowski, M., Jr.; Frost, B. J.; Li, L.; Seeram, N. P. Organometallic ruthenium complexes with thiosemicarbazone ligands: Synthesis, structure and cytotoxicity of $[(\eta^6\text{-}p\text{-cymene})\text{Ru}(\text{NS})\text{Cl}]^+$ (NS = 9-anthraldehyde). *Inorg. Chem. Commun.* **2009**, *12*, 1094–1098.
- (34) Stringer, T.; Therrien, B.; Hendricks, D. T.; Guzgay, H.; Smith, G. S. Mono and dinuclear ($\eta^6\text{-arene}$) ruthenium(II) benzaldehyde thiosemicarbazone complexes: Synthesis, characterization and cytotoxicity. *Inorg. Chem. Commun.* **2011**, *14*, 956–960.
- (35) Su, W.; Zhou, Q.; Huang, Y.; Huang, Q.; Huo, L.; Xiao, Q.; Huang, S.; Huang, C.; Chen, R.; Qian, Q.; Liu, L.; Li, P. Synthesis, crystal and electronic structure, anticancer activity of ruthenium(II)-arene complexes with thiosemicarbazones. *Appl. Organomet. Chem.* **2013**, *27*, 307–312.
- (36) Yaman, P. K.; Sen, B.; Karagoz, C. S.; Subasi, E. Half-sandwich ruthenium-arene complexes with thiophene containing thiosemicarbazones: Synthesis and structural characterization. *J. Organomet. Chem.* **2017**, *832*, 27–35.
- (37) (a) Demoro, B.; Sarniguet, C.; Sanchez-Delgado, R.; Rossi, M.; Liebowitz, D.; Caruso, F.; Olea-Azar, C.; Moreno, V.; Medeiros, A.; Comini, M. A.; Otero, L.; Gambino, D. New organoruthenium complexes with bioactive thiosemicarbazones as co-ligands: Potential antitrypanosomal agents. *Dalton Trans.* **2012**, *41*, 1534–1543. (b) Demoro, B.; Almeida, R. F. M. D.; Marques, F.; Matos, C. P.; Otero, L.; Pessoa, J. C.; Santos, I.; Rodríguez, Moreno, A. V.; Lorenzo, J.; Gambino, D.; Tomaz, A. I. Screening organometallic binuclear thiosemicarbazone ruthenium complexes as potential antitumor agents: Cytotoxic activity and human serum albumin binding. *Dalton Trans.* **2013**, *42*, 7131–7146.
- (38) Su, W.; Tang, Z.; Li, P.; Wang, G.; Xiao, Q.; Li, Y.; Huang, S.; Gu, Y.; Laid, Z.; Zhange, Y. New dinuclear ruthenium-arene complexes containing thiosemicarbazone ligands: Synthesis, structure and cytotoxic studies. *Dalton Trans.* **2016**, *45*, 19329–19340.
- (39) Sheeba, M. M.; Muthu Tamizh, M.; Farrugia, L. J.; Karvembu, R. Asymmetric hydrogenation of pro-chiral ketones catalyzed by chiral Ru(II)-benzene organometallic compounds containing amino acid based aroylthiourea ligands. *J. Organomet. Chem.* **2017**, *831*, 45–49.
- (40) Vieites, M.; Otero, L.; Santos, D.; Gajardo, D.; Toloza, J.; Figueroa, R.; Norambuena, E.; Olea-Azar, C.; Aguirre, G.; Cerecetto, H.; González, M.; Morello, A.; Maya, J. D.; Garat, B.; Gambino, D. Platinum(II) metal complexes as potential antitrypanosoma cruzi agents. *J. Inorg. Biochem.* **2008**, *102*, 1033–1043.
- (41) Gambino, D.; Otero, L.; Vieites, M.; Boiani, M.; Gonzalez, M.; Baran, E. J.; Cerecetto, H. Vibrational spectra of palladium 5-nitrofuryl thiosemicarbazone complexes: Experimental and theoretical study. *Spectrochim. Acta, Part A* **2007**, *68*, 341–348.

- (42) (a) Rizal, R. M.; Ali, H. M.; Weng Ng, S. 1*H*-Indole-3-carbaldehyde thiosemicarbazone. *Acta Crystallogr., Sect. E: Struct. Rep. Online* **2008**, *64*, o919–o920. (b) Hartinger, C. G.; Dyson, P. J. Bioorganometallic chemistry from teaching paradigms to medicinal applications. *Chem. Soc. Rev.* **2009**, *38*, 391–401.
- (43) Kurzwernhart, A.; Kandioller, W.; Bächler, S.; Bartel, C.; Martic, S.; Buczkowska, M.; Mühlgassner, G.; Jakupec, M. A.; Kraatz, H. B.; Bednarski, P. J.; Arion, V. B.; Marko, D.; Keppler, B. K.; Hartinger, C. G. Structure activity relationships of targeted [Ru^{II}(η^6 -*p*-cymene)] anticancer complexes with flavonol derived ligands. *J. Med. Chem.* **2012**, *55*, 10512–10522.
- (44) Romero-Canelon, I.; Salassa, L.; Sadler, P. J. The contrasting activity of iodido versus chlorido ruthenium and osmium arene azo- and imino pyridine anticancer complexes: Control of cell selectivity, cross resistance, p53 dependence, and apoptosis pathway. *J. Med. Chem.* **2013**, *56*, 1291–1300.
- (45) Krishnamoorthy, P.; Sathyadevi, P.; Cowley, A. H.; Butorac, R. R.; Dharmaraj, N. Evaluation of DNA binding, DNA cleavage, protein binding and in vitro cytotoxic activities of bivalent transition metal hydrazone complexes. *Eur. J. Med. Chem.* **2011**, *46*, 3376–3387.
- (46) Senthil Raja, D.; Bhuvanesh, N. S. P.; Natarajan, K. Biological evaluation of a novel water soluble sulphur bridged binuclear copper(II) thiosemicarbazone complex. *Eur. J. Med. Chem.* **2011**, *46*, 4584–4594.
- (47) Meyer-Almes, F. J.; Porschke, D. Mechanism of intercalation into the DNA double helix by ethidium. *Biochemistry* **1993**, *32*, 4246–4253.
- (48) Raja, D. S.; Paramaguru, G.; Bhuvanesh, N. S. P.; Reibenspies, J. H.; Renganathan, R.; Natarajan, K. Effect of terminal N-substitution in 2-oxo-1,2-dihydroquinoline-3-carbaldehyde thiosemicarbazones on the mode of coordination, structure, interaction with protein, radical scavenging and cytotoxic activity of copper(II) complexes. *Dalton Trans.* **2011**, *40*, 4548–4559.
- (49) Ramachandran, E.; Kalaivani, P.; Prabhakaran, R.; Zeller, M.; Bartlett, J. H.; Adero, P. O.; Wagner, T. R.; Natarajan, K. Synthesis, characterization, crystal structure and DNA binding studies of Pd(II) complexes containing thiosemicarbazone and triphenylphosphine/triphenylarsine. *Inorg. Chim. Acta* **2012**, *385*, 94–99.
- (50) Chaires, N.; Dattagupta, J. B.; Crothers, D. M. Studies on interaction of anthracycline antibiotics and deoxyribonucleic acid: equilibrium binding studies on interaction of daunomycin with deoxyribonucleic acid. *Biochemistry* **1982**, *21*, 3933–3940.
- (51) Mahadevan, S.; Palaniandavar, M. Spectral and electrochemical behavior of copper(II) phenanthrolines bound to calf thymus DNA. [(5,6-dimethyl-OP)₂Cu]²⁺ (5,6-dimethyl-OP = 5,6-dimethyl-1,10-phenanthroline) induces a conformational transition from B to Z DNA. *Inorg. Chem.* **1998**, *37*, 693–700.
- (52) He, J.; Sun, J.; Mao, Z. W.; Ji, L. N.; Sun, H. Phosphodiester hydrolysis and specific DNA binding and cleavage promoted by guanidinium-functionalized zinc complexes. *J. Inorg. Biochem.* **2009**, *103*, 851–858.
- (53) Ivanov, V. I.; Minchenkova, L. E.; Schyolkina, A. K.; Poletayer, A. I. Different conformations of double stranded nucleic acid in solution as revealed by circular dichroism. *Biopolymers* **1973**, *12*, 89–110.
- (54) Karidi, K.; Garoufis, A.; Tshipis, A.; Hadjiliadis, N.; Dulk, H.; Reedijk, J. Synthesis, characterization, in vitro antitumor activity, DNA binding properties and electronic structure (DFT) of the new complex *cis*-(Cl,Cl)[Ru^{II}Cl₂(NO⁺)(terpy)]Cl. *Dalton Trans.* **2005**, *67*, 1176–1187.
- (55) Selvi, P. T.; Palaniandavar, M. Spectral, viscometric and electrochemical studies on mixed ligand cobalt(III) complexes of certain diimine ligands bound to calf thymus DNA. *Inorg. Chim. Acta* **2002**, *337*, 420–428.
- (56) Chauhan, M.; Banerjee, K.; Arjmand, F. DNA binding studies of novel copper(II) complexes containing l-tryptophan as chiral auxiliary: In vitro antitumor activity of Cu–Sn₂ complex in human neuroblastoma cells. *Inorg. Chem.* **2007**, *46*, 3072–3082.
- (57) (a) Wang, F.; Bella, J.; Parkinson, J. A.; Sadler, P. J. Competitive reactions of a ruthenium-arene anticancer complex with histidine, cytochrome c and an oligonucleotide. *JBIC, J. Biol. Inorg. Chem.* **2005**, *10*, 147–155. (b) Govender, P.; Renfrew, A. K.; Clavel, C. M.; Dyson, P. J.; Therrien, B.; Smith, G. S. Antiproliferative activity of chelating N, O and N, N-ruthenium (II)-arene functionalised poly-(propyleneimine) dendrimer scaffolds. *Dalton Trans.* **2011**, *40*, 1158–1167.
- (58) (a) Liu, H. K.; Berners-Price, S. J.; Wang, F. Y.; Parkinson, J. A.; Xu, J. J.; Bella, J.; Sadler, P. J. Diversity in guanine selective DNA binding modes for an organometallic ruthenium-arene complex. *Angew. Chem., Int. Ed.* **2006**, *45*, 8153–8156. (b) Liu, H. K.; Sadler, P. J. Metal complexes as DNA intercalators. *Acc. Chem. Res.* **2011**, *44*, 349–359. (c) Chen, H.; Parkinson, J. A.; Parsons, S.; Coxall, R. A.; Gould, R. O.; Sadler, P. J. Organometallic ruthenium(II) diamine anticancer complexes: Arene nucleobase stacking and stereospecific hydrogen bonding in guanine adducts. *J. Am. Chem. Soc.* **2002**, *124*, 3064–3082.
- (59) Chen, H.; Parkinson, J. A.; Morris, R. E.; Sadler, P. J. Highly selective binding of organometallic ruthenium ethylenediamine complexes to nucleic acids: Novel recognition mechanisms. *J. Am. Chem. Soc.* **2003**, *125*, 173–186.
- (60) Zeglis, B. M.; Pierre, V. C.; Barton, J. K. Metallo intercalators and metallo insertors. *Chem. Commun.* **2007**, *44*, 4565–4579.
- (61) Abou Zied, O. K.; Al-Shihi, O. I. K. Characterization of subdomain IIA binding site of human serum albumin in its native, unfolded and refolded state using small molecular probes. *J. Am. Chem. Soc.* **2008**, *130*, 10793–10801.
- (62) Ramachandran, E.; Thomas, S. P.; Poornima, P.; Kalaivani, P.; Prabhakaran, R.; Padma, V. V.; Natarajan, K. Evaluation of DNA binding, antioxidant and cytotoxic activity of mononuclear Co(III) complexes of 2-oxo-1,2-dihydrobenzo[h]-quinoline-3-carbaldehyde thiosemicarbazones. *Eur. J. Med. Chem.* **2012**, *50*, 405–415.
- (63) Bhattacharyya, M.; Chaudhuri, U.; Poddar, R. K. Evidence for cooperative binding of chlorpromazine with hemoglobin: Equilibrium dialysis, fluorescence quenching and oxygen release study. *Biochem. Biophys. Res. Commun.* **1990**, *167*, 1146–1153.
- (64) Feng, X. Z.; Yang, Z.; Wang, L. J.; Bai, C. Investigation of the interaction between acridine orange and bovine serum albumin. *Talanta* **1998**, *47*, 1223–1229.
- (65) Raja, D. S.; Bhuvanesh, N. S. P.; Natarajan, K. A novel water soluble ligand bridged cobalt(II) coordination polymer of 2-oxo-1,2-dihydroquinoline-3-carbaldehyde (isonicotinic)hydrazone: Evaluation of the DNA binding, protein interaction, radical scavenging and anticancer activity. *Dalton Trans.* **2012**, *41*, 4365–4377.
- (66) Miller, J. N. Recent advances in molecular luminescence analysis. *Proc. Anal. Div. Chem. Soc.* **1979**, *16*, 203–208.
- (67) Tang, J. H.; Luan, F.; Chen, X. G. Binding analysis of glycyrrhetic acid to human serum albumin: Fluorescence spectroscopy, FT-IR, and molecular modeling. *Bioorg. Med. Chem.* **2006**, *14*, 3210–3217.
- (68) Rahman, K. N. A.; Haribabu, J.; Balachandran, C.; Bhuvanesh, N. S. P.; Karvembu, R.; Sreerkanth, A. Copper, nickel and zinc complexes of 3-acetyl coumarin thiosemicarbazone: Synthesis, characterization and in vitro evaluation of cytotoxicity and DNA/protein binding properties. *Polyhedron* **2017**, *135*, 26–35.
- (69) (a) An, H. W.; Qiao, S. L.; Hou, C. Y.; Lin, Y. X.; Li, L. L.; Xie, H. Y.; Wang, Y.; Wang, L.; Wang, H. Self-assembled NIR nanovesicles for long-term photoacoustic imaging. *Chem. Commun.* **2015**, *51*, 13488–13491. (b) Naeye, B.; Deschout, H.; Roding, M.; Rudemo, M.; Delanghe, J.; Devreese, K.; Demeester, J.; Braeckmans, K.; De Smedt, S. C.; Raemdonck, K. Hemocompatibility of siRNA loaded dextran nanogels. *Biomaterials* **2011**, *32*, 9120–9127. (c) Purkait, K.; Chatterjee, S.; Karmakar, S.; Mukherjee, A. Alteration of steric hindrance modulates glutathione resistance and cytotoxicity of three structurally related Ru^{II}-*p*-cymene complexes. *Dalton Trans.* **2016**, *45*, 8541–8555.

(70) Arun, Y.; Saranraj, K.; Balachandran, C.; Perumal, P. T. Synthesis, anticancer and molecular docking studies. *Eur. J. Med. Chem.* **2014**, *74*, 50–64.

(71) Balachandran, C.; Sangeetha, B.; Duraipandiyan, V.; Karunai Raj, M.; Ignacimuthu, S.; Al-Dhabi, N. A.; Balakrishna, K.; Parthasarathy, K.; Arulmozhi, N. M.; Valan Arasu, M. A flavonoid isolated from *Streptomyces* sp. (ERINLG-4) induces apoptosis in human lung cancer A549 cells through p53 and cytochrome c release caspase dependant pathway. *Chem.-Biol. Interact.* **2014**, *224*, 24–35.

(72) Bennett, M. A.; Huang, T. N.; Matheson, T. W.; Smith, A. K. (η^6 -hexamethylbenzene) ruthenium complexes. *Inorg. Synth.* **2007**, *21*, 74–78.

(73) (a) Haribabu, J.; Jeyalakshmi, K.; Arun, Y.; Bhuvanesh, N. S. P.; Perumal, P. T.; Karvembu, R. Synthesis, DNA/protein binding, molecular docking, DNA cleavage and *in vitro* anticancer activity of nickel(II) bis(thiosemicarbazone) complexes. *RSC Adv.* **2015**, *5*, 46031–46049. (b) Balachandran, C.; Haribabu, J.; Jeyalakshmi, K.; Bhuvanesh, N. S. P.; Karvembu, R.; Emi, N.; Awale, S. Nickel(II) bis(isatin thiosemicarbazone) complexes induced apoptosis through mitochondrial signaling pathway and G0/G1 cell cycle arrest in IM-9 cells. *J. Inorg. Biochem.* **2018**, *182*, 208–221.

(74) Subarkhan, M. K. M.; Ramesh, R. Ruthenium(II) arene complexes containing benzhydrazone ligands: Synthesis, structure and antiproliferative activity. *Inorg. Chem. Front.* **2016**, *3*, 1245–1255.

(75) Jeyalakshmi, K.; Haribabu, J.; Balachandran, C.; Bhuvanesh, N. S. P.; Emi, N.; Karvembu, R. Synthesis of Ru(II)-benzene complexes containing aroylthiourea ligands, and their binding with biomolecules and *in vitro* cytotoxicity through apoptosis. *New J. Chem.* **2017**, *41*, 2672–2686.

(76) Sheeba, M. M.; Muthu Tamizh, M.; Farrugia, L. J.; Endo, A.; Karvembu, R. Chiral (η^6 -*p*-cymene)ruthenium(II) complexes containing monodentate acylthiourea ligands for efficient asymmetric transfer hydrogenation of ketones. *Organometallics* **2014**, *33*, 540–550.

(77) (a) Becke, A. D. Density functional thermochemistry. III. The role of exact exchange. *J. Chem. Phys.* **1993**, *98*, 5648–5652. (b) Lee, C.; Yang, W.; Parr, R. G. Development of the Colle-Salvetti correlation energy formula into a functional of the electron density. *Phys. Rev. B: Condens. Matter Mater. Phys.* **1988**, *37*, 785–789.

(78) (a) Miertus, S.; Scrocco, E.; Tomasi, J. Approximate evaluations of the electrostatic free energy and internal energy changes in solution processes. *Chem. Phys.* **1981**, *55*, 117–129. (b) Miertus, S.; Tomasi, J. *Chem. Phys.* **1982**, *65*, 239–245. (c) Cossi, M.; Barone, V.; Cammi, R.; Tomasi, J. Ab initio study of solvated molecules: A new implementation of the polarizable continuum model. *Chem. Phys. Lett.* **1996**, *255*, 327–335.

(79) Frisch, M. J.; Trucks, G. W.; Schlegel, H. B.; Scuseria, G. E.; Robb, M. A.; Cheeseman, J. R.; Scalmani, G.; Barone, V.; Mennucci, B.; Petersson, G. A.; Nakatsuji, H.; Caricato, M.; Li, X.; Hratchian, H. P.; Izmaylov, A. F.; Bloino, J.; Zheng, G.; Sonnenberg, J. L.; Hada, M.; Ehara, M.; Toyota, K.; Fukuda, R.; Hasegawa, J.; Ishida, M.; Nakajima, T.; Honda, Y.; Kitao, O.; Nakai, H.; Vreven, T.; Montgomery, J. A.; Peralta, J. E.; Ogliaro, F.; Bearpark, M.; Heyd, J. J.; Brothers, E.; Kudin, K. N.; Staroverov, V. N.; Kobayashi, R.; Normand, J.; Raghavachari, K.; Rendell, A.; Burant, J. C.; Iyengar, S. S.; Tomasi, J.; Cossi, M.; Rega, N.; Millam, J. M.; Klene, M.; Knox, J. E.; Cross, J. B.; Bakken, V.; Adamo, C.; Jaramillo, J.; Gomperts, R.; Stratmann, R. E.; Yazyev, O.; Austin, A. J.; Cammi, R.; Pomelli, C.; Ochterski, J. W.; Martin, R. L.; Morokuma, K.; Zakrzewski, V. G.; Voth, G. A.; Salvador, P.; Dannenberg, J. J.; Dapprich, S.; Daniels, A. D.; Farkas, O.; Foresman, J. B.; Ortiz, J. V.; Cioslowski, J.; Fox, D. J. *Gaussian 09, Revision D.01*; Gaussian, Inc., Wallingford, CT, 2009.